Review Article

Dmitriy V. Likhachev*

Certain topics in ellipsometric data modeling with splines: a review of recent developments

https://doi.org/10.1515/aot-2022-0006
Received March 9, 2022; accepted April 22, 2022;
published online July 4, 2022

Abstract: Dielectric function representation by a variety of polynomial spline functions provides a consistent and efficient method for accurate modeling of the material optical properties in the context of spectroscopic ellipsometry data interpretation. Splines as an elegant and purely mathematical way for such modeling task were introduced about three decades ago. In the following years the use of splines in the area of ellipsometric data analysis became widely utilized. The goal of this review is to provide a self-contained presentation on the current status of the dielectric function modeling by splines for advanced industrial ellipsometry users but, hopefully, it can be useful for some scholarly users as well. It is also intended to promote more extended recognition of the spline-based modeling among optical metrology professionals. Here, a brief description of different ways, – ordinary polynomials, piecewise polynomials (splines), and B(asis)-spline functions, – is presented to parameterize an arbitrary function which can be used as an analytic representation of the dielectric-function curves. A number of particular polynomial-based models for the optical functions of materials and how they may be used in applications are also discussed. Particular attention is paid to different concepts of the efficient and optimal spline construction.

Keywords: data analysis; dielectric function; optical modeling; parameterization; spectroscopic ellipsometry; spline functions.

1 Introduction

Spectroscopic ellipsometry (SE) is a non-destructive technique for fast and informative characterization of surfaces, thin films and multilayer structures including not only the film thicknesses but also the optical functions (yet, as of old, often referred to as optical constants) as well as surface and interfacial roughness [1–3]. It is well known that the optical properties of materials are related to the material electronic structure which is, in fact, can be explicitly affected by multiple factors and, therefore, these influencing factors can be characterized based on the analysis oof the measured optical properties. Thus, it is not surprising that SE, which possesses a broad amount of technlogical capabilities, has become so popular not only in the labs around the globe but for routine process monitoring and control in the modern nanoscale electronic and photonic manufacturing industries. In the era of escalation of fabrication challenges and, therefore, increasing complexity of ellipsometric applications, we regularly face various complications in the analysis of optical measurements and extraction of useful information, especially in modern nanotechnology related applications. One of the primary reasons is that the SE, due to its *indirect* nature, suffers an unwanted vulnerability to almost always required optical modeling and dielectric function parameterization.

In this connection, the typical complications encountered in ellipsometric data analysis involve an accurate modeling of the complex dielectric function (DF) $\varepsilon = \varepsilon_1 - i\varepsilon_2$ (or the complex index of refraction $N = n - ik$) of the materials contained in the samples under investigation. Indeed, the DF (or the refractive index) has to be described not only over the appropriate spectral range but also its model should be flexible enough to take account of numerous factors influencing the electronic structure of materials used in nanoscale science and technology (as, for instance, the process conditions, film thickness, composition, stress, defects, quantum effects, etc.).

There are several approaches [1–5] for an adequate DF representation including (1) tabulated optical functions which are often called “dispersion tables”, (2) certain empirical dispersion formulae valid over a restricted spectral interval (Cauchy, Sellmeier, Schott, Hartmann, etc.), (3) oscillator-based optical functions developed from physical principles (Lorentz, Drude, Gaussian, critical

***Corresponding author: Dmitriy V. Likhachev**, GlobalFoundries Dresden Module One LLC & Co. KG, Wilschdorfer Landstr. 101, D-01109 Dresden, Germany, E-mail: dmitriy.likhachev@globalfoundries.com.
https://orcid.org/0000-0002-9842-528X

point, etc.), and (4) multi-component mixture of individual components (effective medium approximation, EMA).

About three decades ago, an elegant and purely mathematical approach to describe the optical functions by various splines came to be recognized as a distinct, useful and practical alternative. Formally, the splines are piecewise polynomial functions of some degree smoothly and continuously "glued" together at the joining points, the abscissas of which are called "knots" or "break-points".[1] Historically, the problem of best approximation of a certain function (curve) or a set of data points has been mainly examined by use of algebraic and trigonometric polynomials. A spline approximation of complex curves (and surfaces, in general) as a mathematical subject was first introduced in the prominent work of Prof. Isaac Jacob Schoenberg, the "Father of Splines", in 1946 [6, 7], but has become a popular tool in various branches of applied mathematics and in the automotive and aircraft industries only in the early 1960s. Thus, before the advent of high-speed computers, neither spline advantage of combining piecewise polynomials nor their good accuracy of approximation were properly valued and, metaphorically speaking, this approach has stayed in a "dormant" state for practical applications for so many years, waiting for someone to finally come up with a punch card. With the coming of the computer era, splines became widely utilized not only in approximation theory, numerical analysis, statistics, computer graphics and geometric modeling but the potential of splines is much greater and they are also used in different engineering and scientific disciplines for describing miscellaneous physical processes in mechanics, thermo- and electrodynamics, atomic and molecular physics, signal processing, etc.

Usually, in more mathematically-oriented texts, the following primary categories for the spline applications are declared:

(1) approximation of a function: for a certain given continuous real-valued function $f(x)$, defined on an interval $[a, b]$, find a simpler, or approximate, function $g(x)$ to minimize the deviation $||f - g||$ (for instance, $||f - g|| = \max_{x\in[a,b]} |f(x) - g(x)|$, the Chebyshev norm) and quantitatively estimate the introduced error;
(2) interpolation of a discrete function: if function $f(x)$ is known at discrete values x_i, then the interpolation derives a continuous function $g(x)$ which passes through all the given data points x_i and estimates $g(x)$ for arbitrary x, – the simplest case is a piecewise *linear* interpolation of a given set of data points;
(3) smoothing and trending a data set (regression): if function $f(x)$ is defined by its discrete values with some noise but it is known that $f(x)$ possesses the property of "smoothness", then one can find an approximating function $g(x)$ for which the deviation $f - g$ is minimal, – such "data smoothing" can be used to help predict trends.

However, the splines used in ellipsometric data analysis can be conceptually assigned to a different category, which we perhaps should simply call "spline representation of the dielectric function". In some sense, the dielectric function representation by splines is a kind of patchwork of all three declared tasks. It is related to the regression since in ellipsometric analysis we try to reconstruct indirectly, via certain calculations, various properties of measured structures by fitting the measured quantities. Also, it is essentially close to the function approximation since we replace a "true", and predominantly unknown, dielectric function by easily computable and smoothing approximation. Finally, since the whole ellipsometric inversion is performed on a given discrete set of data points, in fact, to compute the function values at any desired points, one should accomplish the function interpolation. It is now widely acknowledged that the dielectric function representation by splines is an extremely useful means of the DF modeling. Spline functions are attractive for a number of reasons. One of the obvious advantages to utilize various kinds of spline functions is that often there is no need for the DF parameterization by typical physics-based oscillator models and many applications, especially in industrial metrology, can be developed using spline curves for determining the optical functions of materials. Other examples of the spline benefits for ellipsometric data modeling will be highlighted throughout the review.

The objective of this paper is to provide a self-contained presentation on the current status of the DF modeling by spline functions for advanced industrial ellipsometry users but, hopefully, it can be useful for some scholarly users as well. The outline of this review is as follows. We provide first, in Section 2, a very brief description

1 Before the widespread use of computer-aided design tools, drawing of smooth and precise curved objects for shipbuilding, airplane manufacturing and the like has required use of real physical objects, – for instance, a thin flexible strip of a material (wood, steel or plastic) called a "spline" (see its use by a Boeing engineer on one of the exclusive illustrations from Prof. Carl de Boor's web page http://pages.cs.wisc.edu//~deboor/draftspline.html; accessed January 11, 2022). A draftsman used to draw a smooth and "pleasing to the human eye" curve by placing a physical spline on a piece of Whatman's drawing paper, holding it at specified places with special hooked lead weights called "ducks" (or "whales") and drawing along the spline with a pencil.

of different ways, namely, ordinary polynomials, piecewise polynomials (splines), and B(asis)-spline functions, to parameterize an arbitrary function which can be used as an analytic representation of the (ε_1, ε_2) curves. Section 3 is devoted to the polynomial-based modeling of the optical functions of materials for use in further SE data fitting although, for the sake of justice, it is necessary to notice that initially the splines of various types have been used for smoothing the dielectric spectra after the "point-by-point" fitting and also for storing the dielectric functions in ellipsometry software databases. At first, we briefly review the natural-cubic-spline representation as well as highly sophisticated critical-point parametric dispersion models developed to describe the complex-shaped dielectric functions. Then the parameterization of the dielectric function by means of B-splines is discussed in some details as the most adopted spline approach in ellipsometric data analysis. It should be especially emphasized that the actual performance of the B-spline parameterization in practical applications strongly depends on the number and locations of knots used to describe the dielectric function. Therefore, Sections 4 and 5 deal with several guidelines for selection of optimal knot numbers and their appropriate locations to achieve better modeling accuracy in SE data analysis. The penalized B-spline (P-spline) approach for the dielectric function modeling, which we can also identify as an area of future research, is outlined in Section 6. Finally, we end with a bibliography of selected publications on the review's topic.

2 Spline preliminaries

As we already mentioned in Section 1, the task of the dielectric function representation by splines is partly related to an interpolation of a discrete function since in SE the measured data are collected at multiple discrete wavelengths λ (photon energies E) over a broad spectral range. Typically, the SE data are represented by ellipsometric angles Psi (Ψ) and Delta (Δ) (or tan(Ψ) and cos(Δ)) at each measured wavelength and angle of incidence. These two measured quantities Ψ and Δ can be used to determine, via direct inversion or model-based regression, the material properties, i.e., the real and imaginary parts of DF ε, or the complex index N. A conventional approach employs an explicit parameterization of the $\varepsilon_2(E)$ spectrum of a material and then $\varepsilon_1(E)$ is analytically or numerically derived using the Kramers–Kronig (K–K) relation [8] that couples the real and imaginary parts of the complex dielectric function:

$$\epsilon_1(E) - 1 = \frac{2}{\pi} P \int_0^{\infty} \frac{E' \epsilon_2(E')}{E'^2 - E^2} \mathrm{d}E', \tag{1}$$

where P denotes the principal value of the integral. For another K–K relation, which expresses $\varepsilon_2(E)$ via $\varepsilon_1(E)$, see [8]. A comprehensive overview of this procedure can be found elsewhere [1–5].

General representation of a given continuous function can be written as a linear combination of some weighted basis functions

$$S(x) = \sum_{k=0}^{n} a_k \varphi_k(x), x \in \mathbb{R}, \tag{2}$$

where n is the number of basis functions φ_k, a_k represents the real coefficient for the kth basis function. Here, we briefly remind the reader of general background material regarding different ways to parameterize an arbitrary function by some quite reasonable functional forms.

2.1 Polynomial representation

Ordinary polynomials are well known for their important role in the approximation of functions, integrals and derivatives, in the solutions of equations, etc. Polynomials may be considered as a special case of splines *with no knots*. The polynomial representation occurs when the basis functions φ_k in Equation (2) take the form

$$\varphi_k(x) = x^k, \tag{3}$$

that is, $\varphi_0 = 1$, $\varphi_1 = x$, $\varphi_2 = x^2$,… Therefore, a polynomial of degree n, where n is a non-negative integer, may be expressed in more common form

$$\begin{aligned} p_n(x) &= \sum_{k=0}^{n} a_k x^k \\ &= a_0 + a_1 x + a_2 x^2 + \cdots + a_{n-1} x^{n-1} + a_n x^n \end{aligned} \tag{4}$$

(note that there are $n + 1$ polynomial coefficients a_k).

Famous Weierstrass's approximation theorem [9] states that any function continuous on the interval [a, b] can be approximated uniformly by polynomials to any degree of accuracy:

$$\lim_{n \to \infty} \left(\max_{x \in [a,b]} \left| f(x) - p_n(x) \right| \right) = 0. \tag{5}$$

Furthermore, polynomials have a simple form and they are intuitive and quite easy to work with. These and some other advantages have made polynomials very useful and popular tool in a staggering variety of applications, ranging from physics, chemistry, engineering to statistics,

economy, finance, – even traffic control and medical imaging, – i.e., wherever one needs to model many kinds of real-world situations.

Unfortunately, "everything has its drawbacks…" [10] and the polynomial representation is not always efficient and, in practice, can behave poorly even for slowly varying and analytic over the whole interval functions. A classical example of such disadvantage is a well-known Runge's phenomenon [11] which occurs when smooth functions are interpolated by polynomials of increasing degree *on equally spaced* (equidistant) grids. In his numerical example, Carl Runge showed that if the analytic for all real x function $f(x) = (1 + x^2)^{-1}$ (the Runge function) is interpolated with evenly spaced points in the interval $x \in [-5,5]$, then $p_n(x) \to f(x)$ only if $|x| < x_c \approx 3.63$ and diverges for larger $|x|$, that is, a problem of oscillations at the interval's edges arises. However, in order to model complex-structured functions or data sets, one may need to increase the polynomial degree n higher and higher which may result in unpleasant consequences in many cases and produce highly erroneous models. Shown in Figure 1 is an example of undesired oscillating behavior of an ordinary polynomial used to describe the results of spot-size characterization for a normal-incidence spectroscopic reflectometer. Measurements were performed on a series of test pads of various sizes (15–100 μm) formed on a semiconductor wafer. Data analysis includes fitting of an appropriate optical model to measured spectra and monitoring the quality of fit (goodness of fit). As one can see, moving towards smaller test-pad sizes, we observe clear degradation of the fit quality. The example of polynomial non-convergence, or the Runge phenomenon, is certainly evident in the neighborhood of the end points (Figure 1).

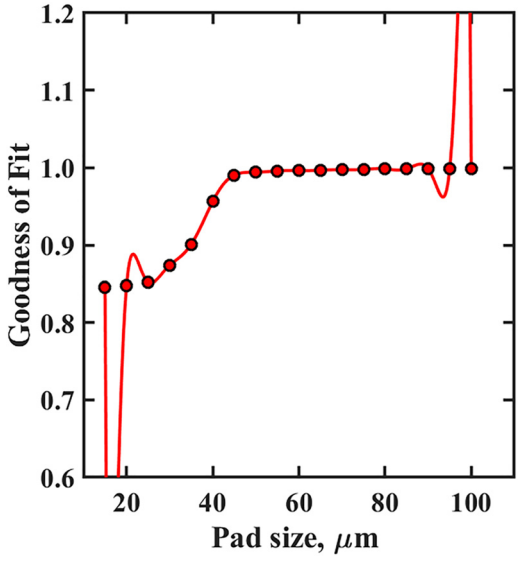

Figure 1: Illustration of the non-convergence for 17-degree polynomial function (red solid line) on equally spaced grid. The red-filled circles denote the quality of fit, taken as dimensionless, in data analysis.

A common example of the polynomial representation used in SE is the Cauchy dispersion formula for the refractive index n (= Re(N)) of insulators or semiconductors in their range of transparency (that is, the extinction coefficient $k \simeq 0$) [1–3, 5] when it is written in terms of the frequency of light ν

$$n(\nu) - 1 = A + B\nu^2 + C\nu^4 + D\nu^6 + \cdots \tag{6}$$

or photon energy $E = h\nu$ (h is the Planck constant)

$$n(E) - 1 = A + BE^2 + CE^4 + DE^6 + \cdots, \tag{7}$$

where A, B, C, and D are the material-dependent Cauchy coefficients. Since the Cauchy relationship is, in fact, an semi-empirical model (although it can be derived from a classical Lorentz oscillator model by assuming zero damping; see, for instance, Ref. [2], p. 170) which assumes $k = 0$ and, therefore, the model is not Kramers–Kronig consistent. Note that the Cauchy dispersion formula in form of Equation (6) is conceptually different from the similar-looking Buchdahl model $n = n_0 + a_1\omega + a_2\omega^2 + \cdots + a_q\omega^q$ [12] which also approximates the dispersive properties by polynomials but only in terms of so-called *chromatic coordinates* $\omega(\lambda) = (\lambda - \lambda_0)/(1 + \alpha(\lambda - \lambda_0))$, where λ_0 is a suitably chosen base (or reference) wavelength and α is a certain tuning parameter. Occasionally in the literature, the more traditional form of the Cauchy dispersion relationship, expressed in terms of the wavelength of light λ

$$n(\lambda) = A + \frac{B}{\lambda^2} + \frac{C}{\lambda^4}, \tag{8}$$

is also referred as a "polynomial equation" or "polynomial model." However, such naming practice should be considered as a violation of the conventional rules since Equation (8), strictly speaking, is not a polynomial because its terms have the negative exponents but the polynomials, by definition, have only non-negative integer exponentiation of variables (here we omit a special case of the Laurent polynomials which allow negative powers of the variable(s) to occur). Therefore, the polynomials as functions have certain properties which the expressions with negative exponents do not manifest, – for instance, the polynomials have no singularities (poles) in contrast with the rational functions in reduced form (like const/λ^{2k} in Equation (8)). In a normal manner, the use of the Cauchy function in form of Equation (6) and (7) as a truncated low-degree polynomial is justified in a limited spectral range

without anomalous dispersion, that is, when the index of refraction starts to decrease toward shorter wavelengths.

2.2 Representation by piecewise polynomials (a.k.a. splines)

As we recalled in the previous subsection, the polynomial representation of sufficiently complex function or over the entire wide interval can be an ill-conditioned task, but locally, on small intervals, even low-degree polynomials can provide a reasonably good approximation. This, then, brings us to the idea of using such polynomials independently of each other to represent certain function in a piecewise manner. Note that we limit ourselves to the univariate polynomial case, that is, a polynomial in a single variable. Incidentally, the use of piecewise polynomials, or splines, dismisses a concern regarding utilization of equally spaced intervals. Therefore, such piecewise representation, or a spline function, consists of polynomial segments defined over each interval of the total range (wavelength or photon energy, for instance) and joined together smoothly at knots. The order of the spline m is the number of polynomial coefficients a_k [see Equation (4)] in the polynomial segments or it is often referred as the polynomial degree n plus one ($m = n + 1$), – for instance, the cubic splines are constructed by third-degree polynomials and, therefore, their order is $m = 4$. The order of spline function determines the smoothness of the piecewise-defined curve since the derivatives up to order $m - 2$ of the adjacent polynomial segments must be equal at joining points. Thus, a spline function is determined by the degree n of the polynomial segments, the polynomial coefficients a_k, and a series of non-descending knot values known as a knot vector $X = \{x_0, x_1, \ldots, x_{l-1}, x_l\}$. Splines arise naturally in many extremal problems in a wide variety of scientific and engineering fields [13–15].

Now, let us take a closer look at the case $n = 3$ ($m = 4$), i.e., the cubic splines, which are the most common choice for many applications since these functions are continuous and they are smooth in the first derivative (slope) and continuous in the second one (curvature). Besides, traditionally the cubic spline functions are reputed so well-behaved, therefore a statistical folklore asserts that "a cubic spline is so smooth that the human eye cannot detect the knots" [16]. Let a given wavelength or energy interval $[a, b]$ be presented by a union of subintervals $[x_0, x_1] \cup [x_1, x_2] \cup \ldots \cup [x_{j-2}, x_{j-1}] \cup [x_{j-1}, x_j], j = 1, 2, \ldots, l$. Assume that over each subinterval $[x_{j-1}, x_j]$ the function can be presented by a third-degree polynomial (as illustrated in Figure 2)

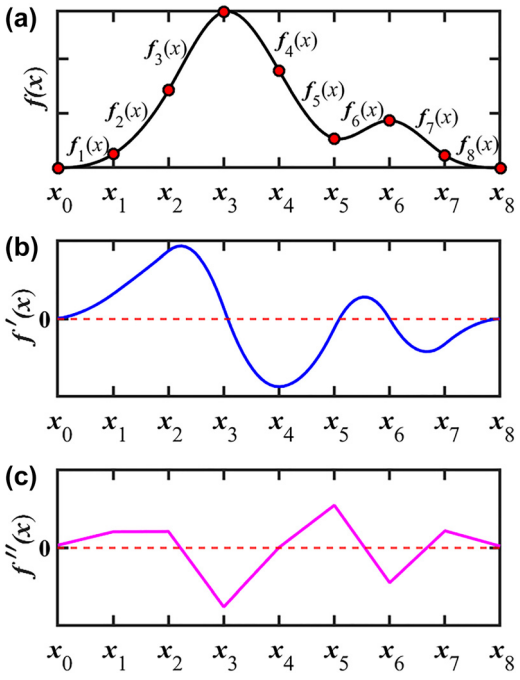

Figure 2: An example of function presented by a third-degree polynomial segments: (a) cubic spline function consisting of eight polynomial segments: here $P: a = x_0 < x_1 < x_2 \cdots < x_7 < x_8 = b$ is a partition (equidistant) of the interval $[a, b]$, $f_1(x)$, $f_2(x)$,…, $f_8(x)$ are the polynomial segments, each described by Eq. (9); (b) the first-order derivative of the spline function: smooth and continuous; (c) the second-order derivative of the spline function shown in (a): not smooth but continuous. Since the spline function $f(x)$ is piecewise cubic, its third-order derivative $f(x)$ is piecewise constant (not shown here).

$$f_j(x) = a_j + b_j(x - x_{j-1}) + c_j(x - x_{j-1})^2 + d_j(x - x_{j-1})^3, x \in [x_{j-1}, x_j], j = 1, 2, \ldots, l. \quad (9)$$

From imposed continuity condition we have the following constraints:

1. at each interior knot the values of adjacent polynomials (splines) must be the same:

$$f(x_j - 0) = f(x_j + 0); \quad (10)$$

2. at each interior knot the values of the first derivatives of adjacent splines must be the same:

$$f'(x_j - 0) = f'(x_j + 0); \quad (11)$$

3. at each interior knot the values of the second derivatives of adjacent splines must be the same:

$$f''(x_j - 0) = f''(x_j + 0). \quad (12)$$

Also, there are different endpoint derivative conditions to get a unique solution for the cubic spline function. For

example, if the second derivatives of the third-degree polynomials are forced to be zero at the endpoints of the interval $[a = x_0, b = x_l]$, i.e., $f''(x_0) = f''(x_l) = 0$, then such a requirement constrains the function to be a straight line outside the interval. The resulting spline function is called the *natural cubic spline*.

Cubic spline representation works well in many cases although it is also not free of certain inconveniences, – to quote Schoenberg [17]: "Polynomials are wonderful even after they are cut into pieces, but the cutting must be done with care." Indeed, the piecewise polynomials are determined by many parameters, that is, the polynomial coefficients a_k, which define the shapes of individual polynomial segments. For instance, for a cubic spline there are $4(r-1)$ coefficients, where r is the total number of knots (the size of the knot vector X). If the interval $[a, b]$ is divided in numerous numbers of subintervals, then the number of parameters can easily become excessive. Of course, in the most general case the degrees of the particular polynomial pieces and the number and positions of the knots may vary in different situations. Moreover, the spline representation with superimposed continuity conditions directly implies a *global* disturbing influence on the curve shape due to any alteration of given data point(s) and all polynomial coefficients must be re-evaluated simultaneously.

About a half of century ago Hiroshi Akima developed a *local* method which is less prone to wiggles in the spline interpolation and produces "visually pleasing" spline curves [18]. The Akima's method uses the piecewise cubic polynomials similar to Equation (9) but it does not impose usual continuity constrain on the second derivative and, in comparison with a cubic spline representation, only the continuous first-order derivative must exist. Instead, it introduces certain "local" procedure to compute the slope $s_j \overset{\text{def}}{=} f'(x_j)$ at the point j using the slopes (m_{j-2}, m_{j-1}) of two preceding segments and the slopes (m_{j+1}, m_{j+2}) of two following segments (see Figure 3) (in other words, the value of the spline function $y = f(x)$ on subinterval $[x_j, x_{j+1}]$ depends only on the function values $y_{j-2} = f(x_{j-2})$, $y_{j-1} = f(x_{j-1})$, $y_j = f(x_j)$, $y_{j+1} = f(x_{j+1})$, $y_{j+2} = f(x_{j+2})$. Then the required slope is calculated as a weighted average of those four nearby slopes:

$$s_j = \frac{|m_{j+1} - m_j| m_{j-1} + |m_{j-1} - m_{j-2}| m_j}{|m_{j+1} - m_j| + |m_{j-1} - m_{j-2}|}, \tag{13}$$

$$m_k = \frac{\Delta y_k}{\Delta x_k} = \frac{y_{k+1} - y_k}{x_{k+1} - x_k},$$

i.e., m_k's are the slopes of line segments $\overline{(j-2)(j-1)}$, $\overline{(j-1)j}$, $\overline{j(j+1)}$, and $\overline{(j+1)(j+2)}$ (Figure 3).

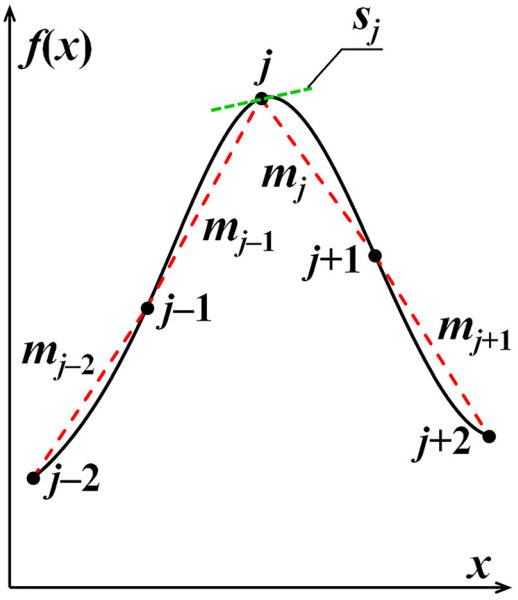

Figure 3: Visualization of the Akima's approach to obtain the slope s_j as a weighted average of the nearest slopes m_{j-2}, m_{j-1}, m_j, and m_{j+1}.

Or this condition can also be presented in more compact form:

$$s_j = \frac{\omega_{j+1} m_{j+1} + \omega_{j-1} m_j}{\omega_{j+1} + \omega_{j-1}}, \tag{14}$$

where $\omega_k = |m_k - m_{k-1}|$ are the corresponding weights. Eventually, moving a point affects only the adjacent portion of the spline curve which is an obvious advantage of the method over ordinary cubic splines. The original Akima's method appoints an equal weighting on both sides of the specified subinterval and also an appropriate treatment of the interval $[a, b]$ end points is required. However, under certain conditions, – for instance, in case when the slopes on the left side are equal (i.e., $m_{j-2} = m_{j-1}$) and the slopes on the right side are also equal ($m_j = m_{j+1}$), – the method requires some modifications. For more comprehensive details concerning the Akima's algorithm improvement, the interested reader is referred to [19–21].

2.3 B-splines, compact support, positivity, and all that (jazz)

Another important spline representation uses a class of functions called B-splines (or B(asis)-spline functions). According to the Curry–Schoenberg theorem, B-splines are not ordinary splines but a set of localized functions from which all other spline functions $S(x)$ can be uniquely built

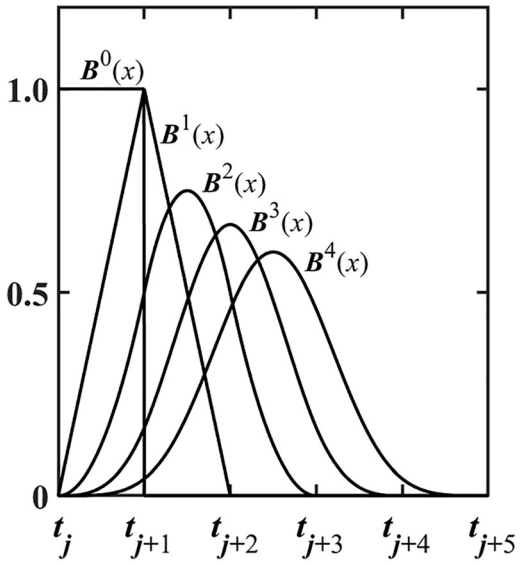

Figure 4: Examples of uniform B-spline basis functions of different degrees.

as a linear combination (weighted sum) of individual basis functions $B^p(x)$ of non-negative integer degree p over certain sequence of knots $T=\{t_0, t_1,\ldots, t_{l-1}, t_l\}$

$$S(x) = \sum_i b_i B_i^p(x), \tag{15}$$

where $i = 0, \ldots, n$, n is the number of basis functions, b_i represents the spline coefficient for $B_i^p(x)$, the ith basis function [22]. In simple phrase, rather than connecting smoothly the local polynomial segments we can form the required spline curve by summation of individual shifted basis functions. Figure 4 shows a few examples of uniform B-spline basis functions of different degrees. A B-spline is called uniform if the knots are equally spaced (equidistant), that is, $\Delta t_j = t_{j+1} - t_j = \text{const}$, and each knot appears only once; otherwise, it is non-uniform. One can see that the basis functions are locally supported piecewise polynomial functions over finite intervals and they are exactly zero outside these intervals, that is, $[t_j, t_{j+p+1}]$ (the *compact support* property). The latter property means that a modification of the spline function $S(x)$ at some point x has only a local influence and will not affect other parts of the function, – in contrast to ordinary piecewise polynomials of the previous subsection, – and this is one of the great advantages of B-spline basis. Note also that the basis functions are non-negative. Therefore, the spline function $S(x)$ in Equation (15) is always positive if all spline coefficients b_i are non-negative (the *convex hull* property). Another important property is that all B-splines with respect to a knot sequence form a *partition of unity*: $\sum_i B_i^p(x) = 1$ for all $x \in [x_p, x_{l-p}]$, where $l+1$ is the number of knots in the knot vector $T=\{t_0, t_1, \ldots, t_{l-1}, t_l\}$ with $l = n+p+1$ (in general, the knot vector can be non-uniform). However, at the knot sequence boundaries the partition of unity property does not hold (Figure 5). All these properties result in a high numerical stability and computation-friendly evaluation of the B-splines. Another interesting fact is that the sequence of normalized and scaled B-splines B^p tends to the Gaussian function as p increases (the *asymptotic convergence* property).

The Cox–de Boor recursion formula [22–24] (sometimes also called the Cox–de Boor–Mansfield recurrence relation) is one of the simplest ways to construct B-splines:

$$B_i^0(x) = \begin{cases} 1, & \text{if } t_j \le x \le t_{j+1} \\ 0, & \text{otherwise} \end{cases}, p = 0,$$

$$B_i^p(x) = \frac{x - t_j}{t_{j+p} - t_j} B_i^{p-1}(x) + \frac{t_{j+p+1} - x}{t_{j+p+1} - t_{j+1}} B_{i+1}^{p-1}(x), p \ge 1. \tag{16}$$

(for some historical comments on the early history of the recurrence relations, see [25]). From Equation (16) we see that a convex combination of two lower-order shifted basis function B_i^{p-1} and B_{i+1}^{p-1} gives the value of the higher-order basis function B_i^p. Figure 6 illustrates that each B-spline of degree p is a linear combination of B-splines of degree $p-1$. One can immediately notice that if a knot multiplicity ξ_j in the knot vector T is equal to one (a knot has multiplicity ξ if it appears ξ times in the knot sequence, i.e., identical knots [26]) the B-spline becomes equal to zero at the end points when $x = t_j$ and $x = t_{j+p+1}$. But for the knots with multiplicity greater than one the recursion can have fractions with zero denominators. Despite the "First Commandment" of

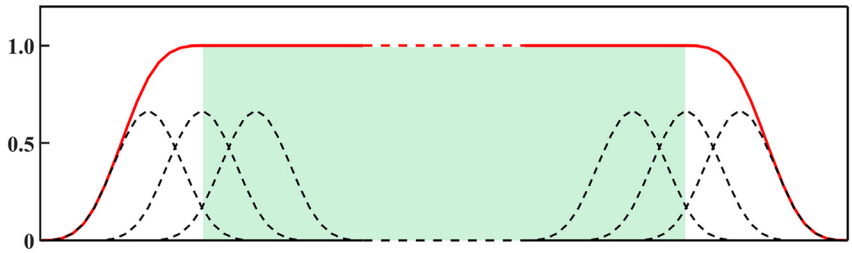

Figure 5: Illustration of the partition of unity property for univariate B-splines: the light-green filled area indicates the natural definition domain where the partition of unity property holds. Red line is formed by linear combination of equally-spaced shifted B-spline basis functions with all coefficients b_i equal to one (shown as black dashed lines).

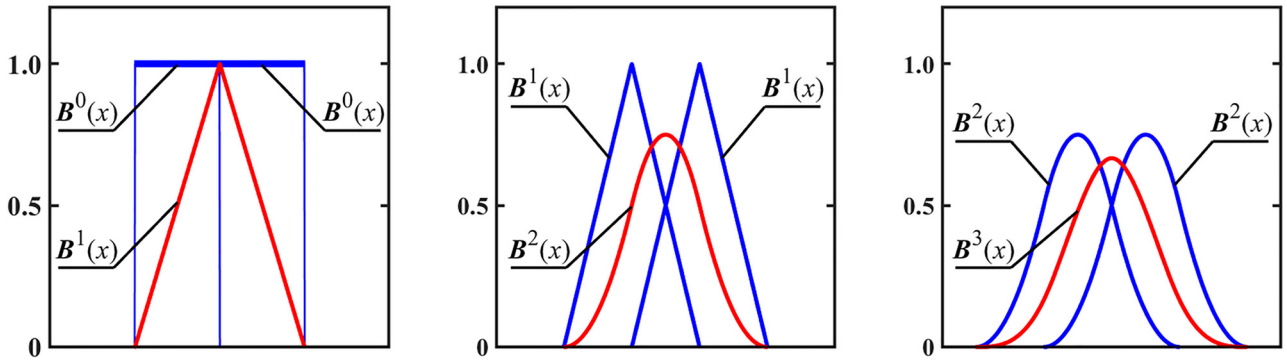

Figure 6: Visualization of the recursively defined B-splines as a combination of two lower-order shifted basis function. (Left panel) Two piecewise constant B-spline basis functions $B^0(x)$ yield a linear ($p = 1$) one (the so-called *hat* function); (middle panel) two linear basis functions $B^1(x)$ form a quadratic ($p = 2$) one; (right panel) two quadratic basis functions $B^2(x)$ produce a cubic ($p = 3$) B-spline.

mathematics "Thou shalt not divide by zero!",[2] in the case of possible divisions by zero in Equation (16) we follow the common convention [26] that "anything divided by zero is zero", allowing, thereby, an incorporation of repeated knots ($\xi > 1$). The knot multiplicity, in fact, controls the continuity of spline function $S(x)$ and its derivatives and increasing the ξ value of a knot reduces the continuity at that knot. For example, a cubic B-spline curve, the most common choice for many applications, with a knot multiplicity $\xi = 4$ is discontinuous at the knot. The knot multiplicity larger than one is a definite advantage in various scientific and engineering fields of computer-aided design, medical imaging, computer vision, advanced animation, geology, oceanography, meteorology, etc. However, the repeated knots must be excluded if there is a strict requirement to enforce an analytical continuity of the spline curve, – as, for instance, for representation of the dielectric function in SE data analysis. Alternatively, B-splines can be defined by means of divided differences. A detailed description of this definition is beyond the scope of this paper, but the interested reader is encouraged to read some of the references available for further information (e.g., [14, 27]).

Besides already mentioned B-spline advantages, like compact support and non-negativity, if a knot vector with predetermined number and locations (not necessary uniform) of knots is used, only the coefficients b_i [see Equation (15)] are considered as tuning parameters which need to be estimated, – as opposed to the standard piecewise polynomials where the number of parameters for each polynomial segment is defined by the polynomial order.

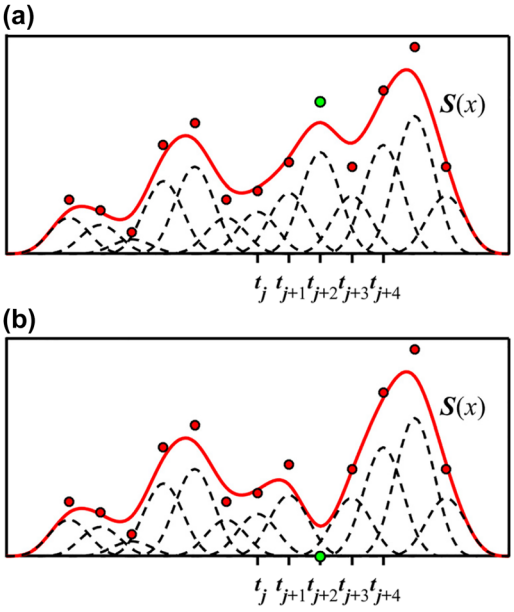

Figure 7: For the sake of simplicity only the uniform cubic B-spline curve $S(x)$ (red solid line) formed by linear combination of shifted B-spline basis functions of degree $p = 3$ (black dashed lines) is shown. The B-spline control points, which can be described as weights for each basis function are visualized by the markers. The green filled marker corresponds to two different control point values of (a) 0.7 and (b) zero. It is not difficult to see that, in that case, the shape of the curve is modified only in the interval $[t_j, t_{j+4}]$.

The coefficients b_i are the ordinates of so-called *B-spline control points* or *de Boor points* (Figure 7). Figure 7 illustrates how the control points affect the individual B-spline basis functions and form the resulting spline curve $S(x)$. It can easily be seen that changing the control points is the most convenient way to modify the shape of the spline curve. Moreover, changing the control point for particular basis function B_i^p affects the spline curve $S(x)$ only on interval $[t_j, t_{j+p+1}]$, i.e., locally. Therefore, the B-spline

2 However, there is a science joke that "…physicists were dividing by zero all the time – as long as no one was looking." [see E. Maor, Thou Shalt Not Divide by Zero!, *Math Horizons* 11 (2003), pp. 16–19. https://doi.org/10.1080/10724117.2003.12021744.

representation of curves is more preferable due to, for instance, computation-friendly mathematical foundation (no need to constrain derivatives or/and curvatures of the concatenated polynomial segments). Finally, the Kramers–Kronig consistent representation of the optical functions (the complex dielectric function and complex index of refraction) by means of B-splines is also possible [28].

One should note that for quite some time the use of B-splines for the function approximation/interpolation have not received a great deal of attention. As has been even pointed out by John Rice, "The B-spline representation has one real drawback; namely, the B-splines are unfamiliar functions. They have a lot of nice properties, but these properties are not trivial to derive. One should view B-splines as new elementary or special functions, analogous to sines or Bessel functions." (see [27], p. 80). Nowadays, this statement regarding a lack of familiarity with the B-splines should be seen as obsolete. Indeed, the advent of so simple and elegant B-spline recursive definition (Equation (16)) has led to a standard and straightforward way for numerical computations in data analysis, computer-aided design and computer graphics applications. The latter ones, particularly in the entertainment industry, are widely familiar even to the general public, – as an example, the morphing transformation of the T-1000 terminator, the liquid-metal man, in James Cameron's *Terminator 2: Judgment Day* is an excellent example of using B-splines: "…All of this stuff was being modeled in uniform cubic b-spline surfaces …" [29].

3 Polynomial-based modeling of the optical functions

This section starts with brief historical remarks concerning primordial use of splines in spectroscopic ellipsometry applications. Then, in Section 3.1, we briefly review the natural-cubic-spline representation as well as highly sophisticated critical-point parametric dispersion models developed to describe the complex-shaped dielectric functions. Finally, in Section 3.2, the parameterization of the dielectric function by means of B-splines is discussed in some details as the most adopted spline approach in ellipsometric data analysis.

3.1 Piecewise polynomial modeling of the dielectric function

In spite of prevalence of the oscillator-based dispersion models [1–5], developed from physical principles, in the last three decades a purely mathematical approach to represent the dielectric functions by means of different categories of spline functions has become increasingly pervasive for the interpretation of spectroscopic ellipsometry data. At first, splines in ellipsometric data analysis were used only for smoothing the dielectric spectra ε (or N) (see, as an example, [30]) after performing point-by-point numerical inversion ([4], pp. 95, 96) which, as it is commonly known, translates existing measurement noise into extracted DF. At about the same time, in works by Vanhellemont et al. [31–33] the dielectric functions (or n and k's), needed for analysis of SE data, were not only smoothed by cubic splines but also stored in ellipsometry software in form of cubic B-splines. This approach provided a few advantages, as it was noted by the authors. First of all, it allows to have a continuous at any wavelength (or photon energy) optical function instead of a tabulated list of n&k's (a.k.a. dispersion table). Moreover, the B-spline representation with just a few corresponding coefficients greatly reduces the consumption of computer memory used for storing the material optical functions, – an important factor for older, low-performing computers. However, it must be clearly stated that in the discussed approach the B-splines and their associated coefficients were not used in regression analysis (data fitting) as fitting parameters, i.e., they were not allowed to vary.

In 1992, Hu et al. [34] developed a Kramers–Kronig consistent dispersion relation for amorphous germanium dioxide GeO_2

$$\epsilon_1(E) = 1 + \frac{A}{\pi}\int_0^{E_1}\left(\frac{E^{\star}\mathrm{e}^{\frac{E-E_1}{E_u}}}{E^{\star 2}-E^2}\right)\mathrm{d}E^{\star} + \frac{A}{\pi}\ln\left(\frac{E_2^2-E^2}{E_1^2-E^2}\right), \qquad (17)$$

where a cubic spline was used for a first time to represent the exponential contribution into the imaginary part ε_2 of the dielectric function, – it allowed to get the resulting integral in analytic form and greatly simplified the data fitting. Strictly speaking, it was not a full spline representation for the dielectric function yet. Later on, this spline-based K–K consistent approach with a natural cubic spline, in more explicit shape, appeared in the paper by Zettler et al. [35] where it was applied to obtain the optical properties of C_{60} fullerene thin film on silicon. The whole spectral range was divided into subintervals at which the imaginary part ε_2 of the dielectric function is represented by cubic polynomial [see Equation (9)].[3] Then the integral

3 Note that in the text of [37] itself the expression for ε_2(E) is incorrectly formulated as a fourth-degree polynomial, a.k.a. *quartic polynomial*, although the resulted integrals, the sum of which forms the K–K integral, were written in correct forms.

in the K–K relation Equation (1) can be approximated (see, e.g., [36], pp. 285–287) as a sum of integrals of the form $\int (x^m/(x^2 - a^2))\,dx$, each one of which can be evaluated analytically ([37], p. 41). In both above-mentioned approaches [34, 35] the associated spline parameters are allowed to vary to adjust ε_2 in a process of regression analysis. We mention, in addition, paper by Zorn et al. [38] in which a combination of the natural cubic spline with unevenly spaced knots and several harmonic oscillators was used to describe different contributions to the dielectric function of indium phosphide (InP).

Furthermore, there are several more instances of piecewise polynomial modeling in ellipsometry data analysis. By way of example, De Sousa Meneses et al. [39] demonstrated the application of a piecewise polynomial dielectric function model to retrieve the DFs of silica and water. In the works of Gilliot et al. [40] and Gilliot [41], the authors proposed the use of "constrained" splines, that is, the piecewise cubic polynomials similar to Equation (9) with certain conditions on the first-order derivatives at knot positions and no constrains on the second derivatives. All these features point generally to an affinity with the Akima's approach. However, in Refs. [40, 41] the expression for the slope at the point j for all interior knots (with one-sided slope estimates for the end points of spectral interval) is written as

$$s_j = \begin{cases} \dfrac{2}{\dfrac{x_{k+1}-x_k}{y_{k+1}-y_k} + \dfrac{x_k-x_{k-1}}{y_k-y_{k-1}}} & \text{if } (y_{k+1}-y_k)(y_k-y_{k-1}) > 0, \\ \dfrac{1}{2}\left(\dfrac{y_{k+1}-y_k}{x_{k+1}-x_k} + \dfrac{y_k-y_{k-1}}{x_k-x_{k-1}}\right) & \text{if } (y_{k+1}-y_k)(y_k-y_{k-1}) < 0, \\ 0 & \text{if } (y_{k+1}-y_k)(y_k-y_{k-1}) = 0. \end{cases} \tag{18}$$

As one can see, Equation (18) represents nothing more than the harmonic mean[4] of the adjacent line segment slopes, that is, $s_j = H(m_{j-1},m_j)$ (cf. Equations (13) and (14) and Figure 3). Although this form of averaging is also legitimate, one should beware of a difference in contribution by larger and smaller slope values in case of the harmonic mean. Namely, the harmonic mean gives a higher weightage to the smaller slopes and *vice versa*.[5] The application of this constrained spline approach has been demonstrated for a series of reference materials as well as ZnO thin films with various morphologies.

There is also an important group of parametric dispersion models to describe the complex-shaped dielectric functions, especially in vicinity of critical points, of poly- and single-crystalline semiconductor materials. Beyond any doubt, these so-called *critical-point (CP) models* deserve our mentioning in a context of this review because some of them use low-order polynomials with Gaussian or Lorentz broadening to describe the dielectric function ε of semiconductors. It is generally accepted that such model was initially introduced by Kim et al. (the Kim–Garland model) and applied to GaAs and $Al_xGa_{1-x}As$ alloys [42, 43]. The use of polynomials makes this model solvable analytically in certain cases. The mathematical details of the Kim–Garland model were also addressed elsewhere [4]. It was noted that an application of the model results in excellent quantitative agreement with experimental results. However, the model is highly complex and contains a large number of variable parameters, – for instance, the authors of work [43] used 37 parameters to get the dielectric function of $Al_xGa_{1-x}As$ alloy for each x and 119 parameters altogether. It is not a surprise that in this case considerable correlations between the model parameters may exist. Nevertheless, the Kim–Garland model gave rise to the so-called *Gauss–Lorentz* oscillator model by replacing the joint density of state function with the Dirac δ-function [44], – the Gauss–Lorentz model allows the broadening of the absorption peak to vary smoothly between the Lorentzian and Gaussian shapes.

Shortly after development of the Kim–Garland model, Herzinger and Johs [45] proposed the parametric semiconductor (PSEMI) oscillator model which represents the dielectric function as a summation of energy-bounded, Gaussian-broadened polynomials and a few poles responsible for contributions into ε_1 (or index n) due to absorption occurring outside the spectral range used in data analysis. Each PSEMI oscillator consists of four smoothly connected polynomial segments: typically, two fourth-order inner polynomials and two second-order outer polynomials (see Figure 8). Such group of polynomials is centered around critical point E_C with corresponding amplitude A_C. At the end points E_L and E_R of each oscillator the polynomials are forced to be equal to zero. The coordinates of two control points (E_{ML}, A_{ML}) and (E_{MR}, E_{MR}) correspond to the joining points of the polynomials. These control points allow essentially independent control of the asymmetric properties of the PSEMI oscillator shape. Moreover, at the energy E_C the model allows the amplitude discontinuity between the left and right polynomials, controlled by an extra

4 *The harmonic mean is the reciprocal of the average of the reciprocals of certain values; see CRC Standard Mathematical Tables and Formulas*, 33rd ed. Boca Raton, FL, U.S.A., CRC Press, 2018, p. 70581.

5 Indeed, considering, as a simple example, the harmonic mean of just two positive real numbers x_1 and x_2 can be expressed as $H(x_1, x_2) = 2/(_1/x_1 + _1/x_2) = 2x_1x_2/(x_1 + x_2) = w_1x_1 + w_2x_2$, where $w_1 = x_2/(x_1 + x_2)$ and $w_2 = x_1/(x_1 + x_2)$. Obviously, if $x_1 < x_2$ when $w1 > w_2$, – thus, the harmonic mean favours *smaller* numbers.

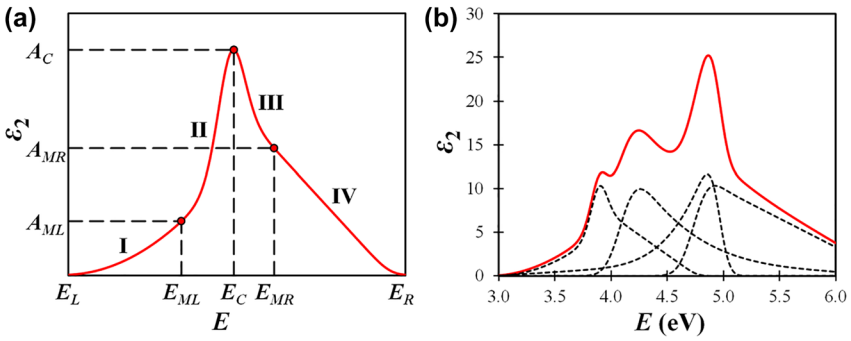

Figure 8: An example of the single PSEMI oscillator and a constructed ε_2 lineshape: (a) A sketch of a single CP structure consisting of four polynomial segments labeled as I, II, III, and IV. This is just one example of the PSEMI oscillator (without possible discontinuity in amplitude at the center energy E_C). (b) As an illustration, four PSEMI oscillators of different shapes (black dashed lines) are summed together to form the imaginary part ε_2 of the DF for a certain hypothetical material (red solid line).

parameter. Thus, the PSEMI oscillator structure is defined by five energies (E_L, E_{ML}, E_C, E_{MR}, and E_R) and three amplitudes (A_{ML}, A_C, and A_{MR}) as well as possible amplitude discontinuity parameter. In addition to that, the model includes the Gaussian broadening factor for each CP. The Herzinger–Johs model does not use the polynomial coefficients *per se* as the fitting parameters. Finally, the full imaginary part ε_2 of the DF can be expressed as a superposition of multiple PSEMI oscillators, that is, the oscillators play a role of *sui generis* "skeleton". Figure 8 also illustrates the ε_2 spectra of a certain fictitious material composed of four separate PSEMI oscillators. The corresponding real part ε_1 of the DF can be obtained through the Kramers–Kronig relation [see Equation (1)]. Detailed mathematical descriptions of the model as well as a comprehensive explanation and discussion of the model parameters are also provided in Ref. [5].

Since its development, the Herzinger–Johs parametric oscillator model has been used in multiple applications and some of them as examples can be found in Refs. [45–53]. However, despite many advantages, such as excellent flexibility in high-fidelity description of the sharp DF features and guaranteed K–K consistency, there are apparent shortcomings as well. In particular, the aforementioned flexibility, determined by a large number of fitting parameters (e.g., the PSEMI model for a silicon substrate contains 58 adjustable internal parameters [46]) and inter-parameter correlations, leads to non-uniqueness of the resulting model. Obviously, it is possible to obtain multiple combinations of model parameters which will result in approximately the same ε_2 curve and, therefore, alike quality of fit in ellipsometric data analysis. In fact, this is not a significant disadvantage since those PSEMI oscillator parameters do not have direct relationship to CP parameters obtained from derivative analysis. Also, due to the model complexity its usage typically requires an expertise from a high-level metrology specialist.

3.2 Parameterization of the dielectric function by means of B-splines

As far as we are aware, the B-spline public debut on the "ellipsometric stage" dates back to works by Vanhellemont et al. [31–33]. As mentioned in the previous subsection, in that case B-splines were employed for smoothing and storing in software the already obtained ε_1 and ε_2 spectra, – and all B-splines coefficients were fixed and not varied during the regression analysis. Next we mention the article by Kuzmenko [54], concerned with the dielectric function representation by a linear superposition of an enormous number of narrow Lorentzians or triangular-shaped functions where the Lorentz oscillator strengths or the coefficients of the triangular functions are the adjustable parameters in the regression analysis. Actually, since the triangular functions are locally supported, i.e., nonzero only inside a small interval, they are more preferable candidates for modeling some real materials like the organic films with numerous and overlapping sharp

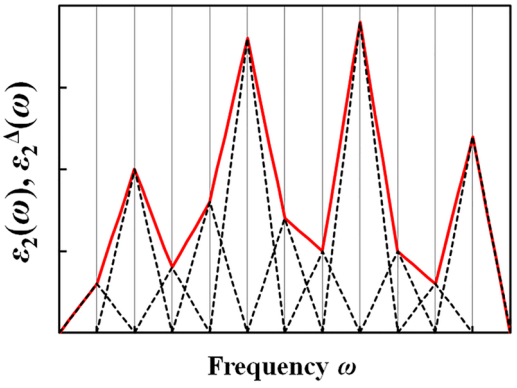

Figure 9: The Kuzmenko's "forest" [54] of several triangular functions (indicated by black dashed lines) as a prototype of the B-spline representation with the basis functions of degree one (cf. Figure 4).

absorption peaks. Then, similar to Equation (2), the imaginary part of ε may be represented by a linear summation of triangular functions $\epsilon_2^{\triangle}$ located at specified grid coordinates (frequencies) as

$$\epsilon_2(\omega) = \sum_i A_i \epsilon_{2,i}^{\triangle}(\omega), \tag{19}$$

where the coefficients A_i are allowed to vary (fitting parameters) and the functions $\epsilon_{2,i}^{\triangle}(\omega)$ play a role of the basis functions:

$$\epsilon_{2,i}^{\triangle}(\omega) = \begin{cases} (\omega - \omega_{i-1})/(\omega_i - \omega_{i-1}), & \omega_{i-1} < \omega \leqslant \omega_i, \\ (\omega_{i+1} - \omega)/(\omega_{i+1} - \omega_i), & \omega_i < \omega < \omega_{i+1}, \\ 0, & \text{otherwise.} \end{cases} \tag{20}$$

The real part can be obtained by the K–K relation Equation (1). The attentive reader will notice that Kuzmenko's approach looks exactly like a prototype of the representation by B-spline basis functions of degree 1, the hat functions (Figure 9). Furthermore, as it has been emphasized in Ref. [54], the frequency grid should be dense enough to accurately represent certain complex-shaped dielectric functions, that is, by using a large number of fixed equally-spaced frequencies (possibly close or even equal to the number of measured spectral points). Obviously, an enormous number of grid points will result in an enormous number of fitting parameters (the coefficients A_i) which may lead to some instability in numerical regression analysis [54]. Moreover, the same procedure was also expanded to magneto-optics (see, for example, Ref. [55]).

In 2008, Johs and Hale [28] proposed to describe the ε_2 curve by means of B-splines of arbitrary order and then the real part ε_1 can be analytically derived using the K–K relation. Formally speaking, such K–K consistent derivation can be abstracted as follows:

By introducing the B-spline representation

$$\epsilon_2(E) = \sum_i b_i B_i^k(E), \tag{21}$$

then

$$\epsilon_1(E) = \epsilon_1(\infty) + \sum_i b_i \phi_i^k(E), \tag{22}$$

where

$$\phi_i^k(E) = \frac{2}{\pi} P \int_0^{\infty} \frac{E' B_i^k(E')}{E'^2 - E^2} \, \mathrm{d}E', \tag{23}$$

which is the K–K transform of the B-spline basis function B_i^k. Johs and Hale also noted that the basis function ϕ_i^k can be represented as

$$\phi_i^k(E) = \frac{1}{\pi}\left(I_i^k(E) + I_i^k(-E)\right), \tag{24}$$

where

$$I_i^k(E) = P \int_0^{\infty} \frac{B_i^k(E')}{E'^2 - E^2} \, \mathrm{d}E' \tag{25}$$

and the integral I_i^k can be computed by the same Cox–de Boor recursion relation Equation (16) (further details can be found in Ref. [28]). Therefore, the problem of data fitting (regression analysis) will be reduced to the determination of the coefficients b_i. This introduction of the recursion formula for I_i^k was a major step towards the fast adoption of the K–K consistent B-spline formulation in SE data analysis.

The B-spline approach for the DF modeling has multiple advantages which follow from definition and properties of the basis spline functions (see Section 2.3 above for details). First of all, such purely mathematical way to express the optical functions of a material does not involve any theoretical models for the material response to light exposure, that is, the interaction of light with material's electronic and ionic subsystems. Also, it is easy to control a sign of the imaginary part ε_2, – since ε_2 ought to be always positive or zero, all spline coefficients must be non-negative. And last, but certainly not least, the B-spline modeling is now available as an option in some ellipsometric software packages which accompany various commercial spectroscopic ellipsometers. Evidently that in the last decade or so this approach has been gaining popularity within the ellipsometric community because our search in the *Google Scholar* database with combination of the keywords "B-spline" AND "spectroscopic ellipsometry" (here AND means the Boolean operator) returns more than 700 entries for publications from 2008 to 2021. Certainly, it is not possible to cite all relevant publications on the topic and we provide only a short selection of corresponding references [51, 56–67] for the interested reader, – and we hope that any reader will not be offended if we confess that this choice of works might be slightly subjective and not simply based on the number of the *Google Scholar* citations.

To the best of our knowledge, the first article, in which the Johs–Hale approach to the dielectric function representation by means of B-splines has been used, was published by Weber et al. [56] where it was applied to the hydrogenated amorphous carbon (a-C:H) thin films. Shortly after that, more and more ellipsometry users started using the B-spline parameterization of the optical functions either as a "stepping stone" to more physical modeling (like a summation of Lorentz, Harmonic or/and Gaussian oscillators) or even as a complete alternative to

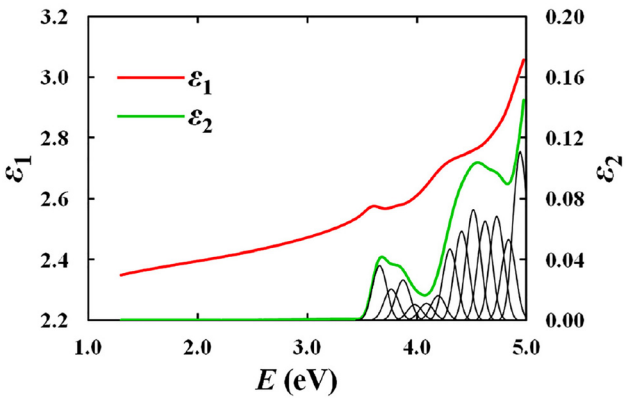

Figure 10: Real (ε_1) and imaginary (ε_2) parts of the complex dielectric function of an ~190 nm-thick E570 resist film parameterized using equally-spaced weighted B-spline basis functions of degree 3 (with small additional contribution at the higher end of the spectral range from outside extra absorption and also assuming the transparent region below 3.25 eV). The individual basis functions forming the ε_2 curve are indicated by thin black solid lines.

commonly used oscillator models. Indeed, after going through many articles on the topic it seems that there is a pronounced tendency to gradually supersede previously widely used point-by-point fitting by the B-spline modeling which maintains the K–K consistency. Although in each particular case one can select the B-spline of any degree p (only constrained by the size of the knot vector $T = \{t_0, t_1, \ldots, t_{l-1}, t_l\}$ and the number of basis functions n since $l = n + p + 1$; see Section 2.3), in practice, the cubic B-splines (with $p = 3$) are the most common choice for many applications since these functions and their first and second derivatives are continuous and, figuratively speaking again, they are "so smooth that the human eye cannot detect the knots" [16]. Or, as Eilers and Marx stated with confidence [68], "In practice there is seldom a need for another value." As an example, Figure 10 demonstrates the complex dielectric function $\varepsilon = \varepsilon_1 - i\varepsilon_2$ of the E570 resist composed from multiple weighted cubic B-spline basis functions. As we have already mentioned, B-splines are commonly used throughout many industrial and scientific applications. As an aside from ordinary ultraviolet–visible–near-infrared (UV–VIS–NIR) ellipsometry/reflectometry, for a very long time B-splines have been also used in optical metrology for data analysis of neutron and X-ray specular reflectivity and reconstruction of scattering-length-density profiles [69–72].

However, turning back to the dielectric function representation by B-splines, we should declare that the approach still is far from being perfect for a number of reasons. Firstly, since the B-spline formulation is not physics-based, an extraction of useful physical information about the material under study, like the energy band gap E_g, is not straightforward and required certain additional ways of evaluation. Another disturbing shortcoming arises from the fact that the actual performance of B-spline parameterization in the regression fit is strongly affected by the choice of knot vector, i.e., the number of knots and their distribution density (uniform or non-uniform). In a simplest case of equally-spaced knots, it is intuitively easy to see that a spline function with fewer knots may not fit some sharp and narrow spectral features (underfitting). On the other hand, increasing the number of knots beyond certain optimal value implies high flexibility but may also put us at risk to overfit the data and, hence, to produce highly noisy or even unphysical results, – some illustrative examples can be found in Refs. [73–75]. Optimal knot allocation is a long-standing issue and it is required to prevent under- and overfitting in SE data analysis. Generally speaking, the problem of overfitting which is attributable to any models, not only the spline ones [76, 77], has been well-recognized in the global community of modelers for quite some time and even referred as "Beware of von Neumann's elephants" [78]. Here we can well afford a brief scientific-historical digression on the origin of the now classic "von Neumann's elephant" wording. The reason lies in the story told by famed theoretical physicist and mathematician Freeman Dyson about his memorable conversation with another brilliant theoretical and experimental physicist Enrico Fermi occurred in the spring of 1953: "In desperation I asked Fermi whether he was not impressed by the agreement between our calculated numbers and his measured numbers. He replied, "How many arbitrary parameters did you use for your calculations?" I thought for a moment…and said, "Four." He said, "I remember my friend Johnny von Neumann used to say, *with four parameters I can fit an elephant, and with five I can make him wiggle his trunk*." [79]. In 2010, Mayer et al. [80] provided the first successful realization of von Neumann's assertion by reconstructing an elephantine shape with four complex numbers and even having a wiggling trunk by using the real part of the fifth parameter.

The main concepts for the number of knots selection and optimal knot distribution are discussed in the next sections.

4 Choosing the optimal number of B-spline knots

The complexity of dielectric function representation by B-splines, i.e., the B-spline model, is substantially determined by the number of knots or, equivalently, the

corresponding spacing between the knots. In practice, the number of knots used in ellipsometric data analysis is chosen and tuned empirically based on quite often ambiguous and intuitive decisions. Again, we would like to emphasize that our goal here is to find an acceptable balance between the quality of model fit to the experimental data with the model complexity which implies, in particular, the number of knots. For that we can consider the B-spline parameterization of ε as just a mathematical model with variable number of model parameters, in this case, the number of knots. A set of the B-spline models with different number of knots will form a collection of so-called *candidate models*. Selection of the "best" model from this set is usually based on a value of χ^2, the biased or unbiased fitting error estimator [1–3] (the term *mean squared error* (MSE) is also very frequently used for the unbiased estimator), as well as the estimations of the cross-correlation coefficients and confidence limits of the best-fitting parameters. Apparently, the fit to the data does get better with increasing number of knots but at a certain moment we will get into a situation when a separation between measurement noise and actual behavior becomes difficult or even impossible. This is directly related to the problem of predictability when an excessive number of model parameters will perfectly describe one set of measured data but will be significantly less efficient for another one. Therefore, we need to come up with certain "good enough solution" to optimize the B-spline complexity or, in other words, perform a model selection, that is, a process of choosing one model from a set of existing candidate models.

Several traditional MSE-based model selection criteria, such as the Akaike information criterion (AIC), the corrected AIC (AICc), and the Bayesian information criterion (BIC), are among the most popular methods to perform model selection task [81]. In terms of the residual sum of squares (RSS) these penalized informational criteria (IC) are defined as

$$\mathrm{IC}_j = n\ln\left(\frac{\mathrm{RSS}_j}{n}\right) + \mu p + C\,, \tag{26}$$

where subscript j corresponds to one of the candidate model from a set, n is the number of data points, i.e., the number of pairs of the ellipsometric angles (Ψ, Δ), the RSS is the sum of the squares of the vertical deviations from each data point to the curve fitted by jth model, p is the number of model parameters (consists of the number of interior knots and other model variables, like film thicknesses), and μ is the penalty term of different kind for various information criteria:

- Akaike information criterion (AIC): $\mu = 2$
- Corrected AIC (AICc): $\mu = 2n/(n - m - 1)$
- Bayesian information criterion (BIC): $\mu = \ln n$.

The constant C can be neglected in model comparison since only the difference in the IC values (scores) and not their absolute values are relevant. Obviously, all candidate models should be fitted to the same set of data. As one can see, Equation (26) enables computation of the AIC, AICc, and BIC scores from standard regression output. Both the AIC and BIC measures have two terms. The first one is a measure of the model lack of fit and can be reduced by increasing the number of parameters p in the model. At the same time, the second term penalizes for the additional parameters in the model and increases with increasing the number of parameters. The model which gives the minimal AIC or BIC score is considered as the best fitting model since it minimizes the difference between the candidate model and the measured data using minimal number of parameters. Clearly, the BIC penalizes for the addition of new parameters more strictly than the AIC due to the presence of $p\ln n$ penalty weight term and, therefore, it tends to select simpler models, i.e., the models with smaller number of parameters (since $\ln n > 2$ for any practicable data sets and BIC $\approx$ AIC for $n = 7$ or 8). Usually, both of these criteria have shown good agreement on the ranking of candidate models which is fairly surprising since these criteria represent very different approaches. The corrected AIC has been introduced in cases when the number of model parameters p is not small compared to the number of data points n and the ordinary AIC sometimes performs poorly selecting models with excessive number of parameters (there is a simple "rule of thumb": the sample size is considered to be small if n/p is less than 40). If n is large relative to p, $n \gg p$, then the correction to original AIC's

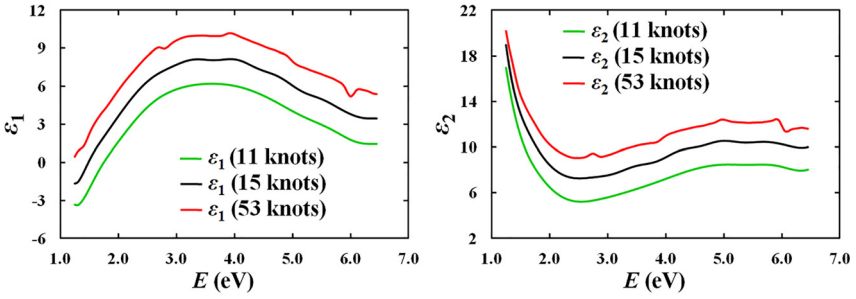

Figure 11: Real (ε_1) and imaginary (ε_2) parts of the complex dielectric function of thin TiN film parameterized by B-splines with different number of equally-spaced knots. To enhance visibility, the curves for 15 and 53 knots are shifted up vertically by 2 and 4 units, respectively.

Table 1: The AICc and BIC results for B-spline parameterization of the TiN dielectric function. The optimal number of knots is determined by the minima of the AICc and BIC measures.

No. of knots	MSE	AICc	BIC
10	5.827	215.1	245.6
12	4.804	200.2	234.6
15	3.817	184.6	224.4
18	3.657	189.3	233.9
27	3.204	207.4	261.9
35	2.911	233.1	289.0

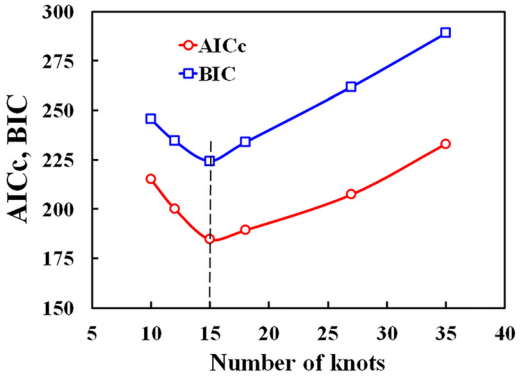

Figure 12: Determination of the optimal number of knots: the AICc and BIC scores are plotted against the number of knots in the B-spline parameterization of the TiN dielectric function. The black dashed vertical line indicates the minima of the AICc and BIC measures.

penalty term becomes negligible and the AICc asymptotically tends to AIC. Due to the differences in the penalty terms, the AIC and BIC measures might disagree from time to time on the ranking of candidate models. In these instances, the IC provides, at least, the upper and lower bounds for the range of suitable models. Moreover, there are a variety of penalized informational criteria, derived within different theoretical frameworks, and a comprehensive overview of mathematical details on the information-theoretic and Bayesian methodology can be found elsewhere [81].

As an example, Figure 11 shows three resulting curves for the real and imaginary parts of the titanium nitride, TiN, dielectric function, obtained with different number of equally-spaced basis knots (11, 15, and 53 knots). Note that the $(\varepsilon_1, \varepsilon_2)$ curves corresponding the B-spline model with 53 knots (the knot spacing was set to 0.10 eV), which yields lowest MSE value of 2.624, exhibit multiple wiggly artifacts due to a small knot spacing. At the same time, the $(\varepsilon_1, \varepsilon_2)$ curves obtained from the model with only 11 knots (the knot step was 0.50 eV) look very smooth but result in the highest misfit with MSE = 5.230. Thus, the reduction of the number of knots in the B-spline model eliminates the observed modeling artifacts but, expectedly, worsens the quality of fit to experimental data, implying that certain essential spectral features might be missed. Therefore, a feasible balance between good fit (low MSE value) and model complexity (to avoid data overfitting) need to be established.

The results of IC analysis of the TiN B-spline parameterization are shown in Table 1 and also plotted in Figure 12 as a function of the number of B-spline knots. These table and figure indicate that the minima of the IC measures (AICc and BIC) occur for 15 equally-spaced knots, – in other words, the criteria point to the B-spline representation with 15 knots as an optimal choice. The $(\varepsilon_1, \varepsilon_2)$ curves generated with optimal number of 15 knots, selected by the information criteria, display the absence of apparent artifacts (see Figure 11) and yield an acceptable MSE value of 3.817.

Certainly, when the AIC and BIC measures select different optimal number of knots, the interpretation of the results might become more sophisticated. More details of the IC analysis as well as other examples are given in Refs. [73, 74, 76, 77].

5 Knot placement matters as well

In the previous section we have detailed one of the possible formalisms for selection of the optimal number of B-spline knots confining ourselves to the case of ordinary equidistant (equally spaced) knots. However, an equidistant knot arrangement is not necessarily an optimal choice, especially if the dielectric function curve of certain material has numerous sharp and overlapping features in some spectral intervals but, *per contra*, is featureless in other regions (see Ref. [66] for a few good examples of B-spline applications in infrared spectroscopic ellipsometry).

Optimal knot placement is a long-standing and challenging problem in the context of non-uniform B-spline approximation. Indeed, the non-equidistant knot allocation would play a key role in order to effectively represent a complex-shaped DF curve. Such “optimized” knot positioning does improve the fit quality for a large variety of the curve shapes with smaller number of knots and by that means reduces the B-spline model complexity [28, 82]. Knot optimization is a popular topic in various areas of scientific and industrial applications such as computer-aided design, image processing, reverse engineering (or shape modeling) material science, etc. and there are too many relevant publications to provide an exhaustive list, therefore, just a few selected recent papers are referenced here [26, 83–87]. In one of conventional ways of dealing

with this problem, the knots are treated as free variables. However, these free-knot splines, i.e., the splines whose knot locations are considered as the parameters estimated from data fitting, suffer from the poor convergency of a multivariate, highly nonlinear optimization problem with multiple local minima of the fitting error estimator (cf. the "lethargy" property [88]). In that case, the performance of local optimization algorithms strongly depends on a rightness of the knot initial choice since the local algorithm will likely "roll down" into the nearest minimum. To avoid such local method drawbacks certain global optimization techniques can be applied but at the expense of high computation costs. Another disadvantage of using free-knot splines is that the resulting knot vector might include identical knots, i.e., knots with multiplicity ξ greater than one which may cause some unwanted features such as discontinuities in the dielectric function curve and/or its derivatives.

Alternative methods for knot allocation involve knot insertion or, on the contrary, knot reduction, i.e., certain iterative processes when we start with an initial knot vector and add new knots or remove certain existing ones and the locations of other knots can be modified as well until some pre-defined criterion on the residual error is satisfied. Usually, an initial vector is chosen as a group of dense knots for the knot removal procedure or a series of rather sparse knots in case of the knot insertion operation. Unfortunately, so far at least as regards the DF spline modeling in ellipsometry, a need for a careful treatment of the optimal knot placement was mentioned rather briefly [5, 28, 40, 41]. For example, Johs and Hale [28] and Gilliot et al. [40, 41] used a multi-iteration knot adjustment as a way to choose optimal knot locations based on the "goodness of fit" between the reference and B-spline modeled dielectric function [28] and the difference between modeled and experimental (Ψ, Δ)-spectra [40, 41]. Very recently, Mohrmann et al. [66] proposed a heuristic "wavelength-range-expansion" algorithm for knot placement with assistance of visual inspection of measured data. However, these methods still may be called as "trial-and-error" procedures and they require direct user intervention and, therefore, are quite subjective, tend to be time-consuming and may not be optimal. An interesting knot insertion approach, guided by the magnitude of error to the target function, has been proposed by Jacobson and Murphy [89]. The approach is based on so-called *force equilibration scheme* where an initial data fit is performed using equidistant knot spacing and a position of each additional knot, inserted into the knot vector on each iteration, has to be estimated from mutual equilibrium between attractive and repulsive "forces" acting on the knot to be added. Those "forces" are defined as a product of a squared error, occurring between the estimated and target curves at certain position, and a distance from this position to the newly added knot. The error function gets updated after inserting each additional knot until final fit is reached. Unfortunately, this technique still allows undesirable redundant knots (knot multiplicity $\xi > 1$) in the knot vector and, therefore, the continuity of the DF curve may be lost or corrupted (see Section 2.3).

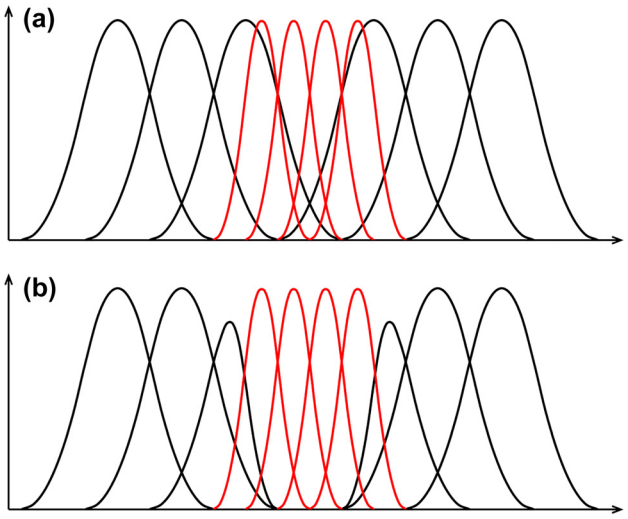

Figure 13: Combination of the coarse (black) and fine (red) grid basis functions of two levels produces the sets of (a) HB- and (b) THB-splines.

Another way of looking at the non-equidistant knot disposition is to implement so-called *hierarchical* B-spline (HB-spline, for short) representation or its improved modification based on truncated hierarchical B-splines (THB-splines) [26, 90–92]. This approach combines several hierarchical levels of equally-spaced fixed knots with different knot resolutions (different knot spacing and/or different spline degree); see Figure 13 for a sketch of 2-level HB-splines (truncated and non-truncated). Since the knots are fixed, the B-spline approximation is actually reduced to a (simple) linear least-squares problem. In case of truncated basis of hierarchical B-splines, the overlap of basis functions at different levels can be decreased. The HB- and THB-splines are locally supported, linearly independent, non-negative and quite well suited for an effective knot placement in different applications [26, 90–92].

When using different, coarse and fine, knot resolutions for the B-spline representation of the dielectric function, we need to set some criterion for the spectral region separation. As shown in Ref. [82], the detection of spectral regions with sharp spectral features in the ε curve can be achieved using the values of the first-order derivative of

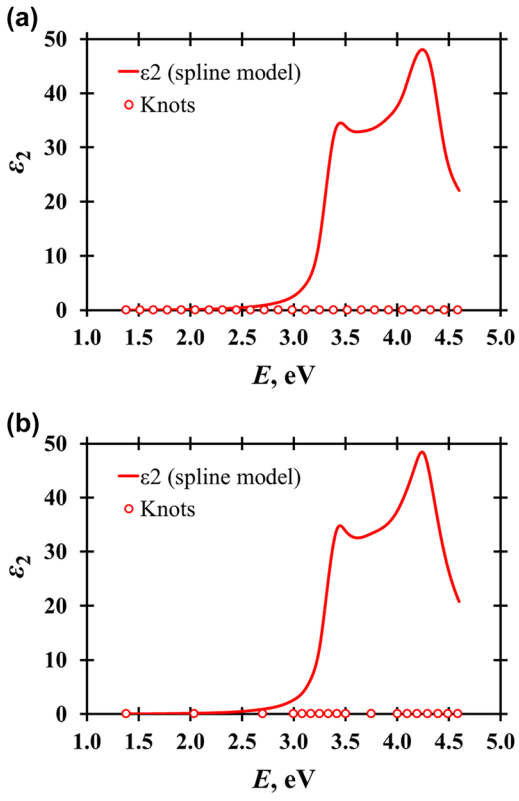

Figure 14: Two B-spline parameterizations of the SOI dielectric function showing the DF imaginary part ε_2 and corresponding spline knot distribution.
(a) an equidistant knot placement for the whole analysis range from 1.4 to 4.6 eV (25 knots, MSE = 1.964); (b) an optimized knot placement with four specially-spaced spectral regions (18 knots, MSE = 1.943) (more details can be found in Ref. [82]).

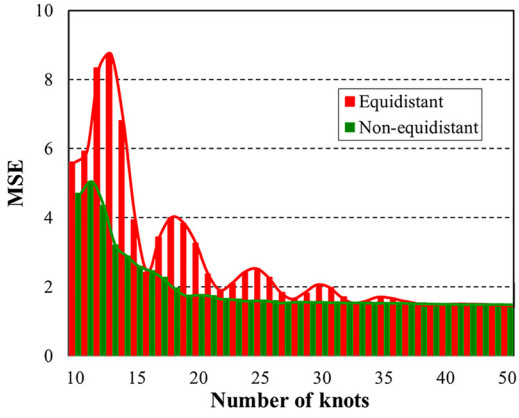

Figure 15: Example of non-monotonic MSE trend from regression fit of ellipsometric data for thin NiSi layer with a uniform B-spline knot distribution; note that non-equidistant knot placement consistently results in a smaller fitting error than conventional way of knot allocation (see more details in Ref. [82]).

some function, to which we refer as a "target DF", ε_{tgt}, obtained from regression data analysis with a "skeleton" of tremendous number of basis functions. The regions with denser knot spacing are defined when the first derivative of the ε_{tgt} curve exceeds a certain predetermined threshold value. Finally, a numerical evaluation for the number of knots for each region is performed by means of a specially introduced measure, the Integral Span (IS), which acts as a peculiar slope-weighting factor and also takes into account the spectral interval width. We will not go much into greater technical detail; please, see Ref. [82] for that. To demonstrate the effectiveness of such, as we all realize, heuristic procedure for composite B-spline knot allocation, it was used to fit the SE data by the B-spline models for the dielectric functions of bulk aluminum, silicon-on-insulator (SOI), and nickel silicide thin films. As an example, the imaginary (ε_2) part of the SOI dielectric function is shown in Figure 14. The SOI optical properties were described using a B-spline model with different number of equidistantly or not-equidistantly distributed knots. As a result, the IS approach consistently outperforms traditional equidistant setup and an acceptable fit is achieved with just 18 optimally-distributed knots (MSE = 1.943) as compared to 25 knots in equidistant arrangement (MSE = 1.964). Another interesting fact, observed in the study, is a non-monotonic MSE descending trend for the case of equally-spaced fixed knot distribution and a presence of well-pronounced MSE fluctuations on a plot of MSE versus total number of knots (Figure 15). The proposed IS-based knot placement scheme is free from such fluctuating behavior. Similar MSE fluctuations in case of the equally-spaced knots were also observed before [89]. The observed MSE fluctuations indicate direct relationship between the type of knot distribution and the accuracy of the B-spline modeling. In some sense, it resembles a discretization error in numerical analysis when a numerical solution depends on a grid quality, that is, resolution, density, etc., of a discrete spatial domain.

There are also a number of other interesting studies demonstrating the use of higher-order derivatives to choose knot locations. For example, in the paper by Conti et al. [93], the authors firstly derive certain smooth "reference function" as a model for the approximate data and the knots of a natural cubic spline are derived using a criterion based on the third-order derivative of the "reference function", – one may note that some sort of an analogy can be drawn between the "reference function" and the "target DF" ε_{tgt} from Ref. [82]. In the recent works by Yeh et al. [85] and Michel and Zidna [86], the authors also have used high-order derivatives for knot vector optimization

("derivative-informed knot placement" as it was refereed in Ref. [87]). Finally, Lenz et al. [87] introduced a Fourier-informed knot placement scheme and also evaluated performance of various combinations of this technique with the derivative-informed method.

In conclusion, we note that everything articulated in this section shows that a search for the optimal knot allocation, no matter how it is performed, is still a hot topic in progress. Obviously, a good knot-placement procedure can provide a considerably better modeling accuracy in SE data analysis. Nevertheless, there is a way to avoid a construction of complex non-equidistant knot vectors and keep using simple evenly-spaced knots. Thereby, a special class of B-splines, so-called *P-splines* (penalized B-splines), with difference-based penalties and its application to the ellipsometric modeling will be discussed in the next section.

6 P-splines as B-splines with roughness penalties in SE analysis

As we already discussed in the previous section, the knot *selection* (not even *adjustment*) problem has been the subject of intensive research for a long time. However, instead choosing the knot positions in one way or another, it is possible to stay with an equidistant grid using a relatively large number of knots and restricting resulted spline curve flexibility by certain roughness penalty. The idea of penalization is not new and can be traced back to, at least, the development of Tikhonov regularization for ill-posed problems [94, 95]. In 1986, O'Sullivan introduced a category of penalized B-splines with a penalty based on the integrated square of the second derivative of the curve [96]. Ten years later, Eilers and Marx eventually published, after three rejections by journals, their manuscript on penalized B-splines with a difference-based penalty [68, 97, 98]. This penalty applies to the B-spline coefficients b_i (see Equation (15)) to ensure that adjoining coefficients do not differ too much from each other in some sense and produce sufficiently smooth fitted curve. There are two important ingredients in using penalized splines to represent the dielectric function: the smoothing (or penalty) parameter and the number of knots, – typically, the knot allocation is simply equidistant, so the problem of optimal knot placement is out of consideration. This is, possibly, one of the primary causes that the authors of the book *"Practical Smoothing: The Joys of P-splines"* [68] declare that *P* in the spline name stands for *practical*.

Mathematically speaking, the smoothing B-spline function $S(x)$ (see Equation (15)) for the dielectric function ε is the function that minimizes the penalized least squares error

$$\sum_j \{\epsilon_j - S(x_j)\}^2 + \alpha \sum_i \left(\Delta^k b_i\right)^2, \tag{27}$$

where the ε_j's are the values of the non-smoothed dielectric function ε_{tgt} at the spectral points x_j, α is the non-negative smoothing parameter which controls the influence of the penalty and may be chosen by certain selection strategy or just a trial-and-error tuning procedure, k is a positive integer, Δ^k is the k-order difference operator defined by means of $\Delta^1 b_i = b_i - b_{i-1}$, $\Delta^2 b_i = \Delta^1(\Delta^1 b_i) = b_i - 2b_{i-1} + b_{i-2}$, $\Delta^k b_i = \Delta^1(\Delta^{k-1} b_i)$ and the first sum is over all measured spectral points x_j. A second-order difference penalty, i.e., $k = 2$, has become a common choice. Other orders of the differences in the penalty can be also used to enforce shape constraints. Eilers and Marx suggested that the number of basis functions can be very large, even larger than the number of data points, – but finite, of course. Thus, this approach also overcomes the problem with optimal selection of the number of knots. This holds due to so-called "power of penalty" property, explicitly formulated in Ref. [98]: "The number of B-splines can be (much) larger than the number of observations. The penalty makes the fitting procedure well-conditioned. This should be taken literally: even a thousand splines will fit 10 observations without problems". However, the truth is that the P-spline approach still is not a magic bullet for SE data analysis since it depends on an extra tuning parameter, namely, the smoothing parameter α, which is the key element of P-splines and must be chosen carefully. Unfortunately, indeed there is no general consensus on how to estimate this parameter although in the numerical analysis literature there are long-lasting discussions on various approaches in order to compute the optimal value of the penalty. The most practical way, of course, is to inspect a wide range of smoothing parameter α and "judge the results visually" (Ref. [68], p. 160). Nevertheless, it will only work for a current set of data and might not be optimal for further data evaluation. Therefore, the determination of parameter α should somehow provide a prediction of yet unmeasured data.

One of the most widely used penalty tuning algorithms is a cross-validation (CV): the simplest for understanding way to check the predictability performance is to select certain trial value of α, remove one data point, perform data fit with selected value of α and then, using the estimated function, predict the value of data point that was removed. Such variant of CV is usually called the "ordinary" or

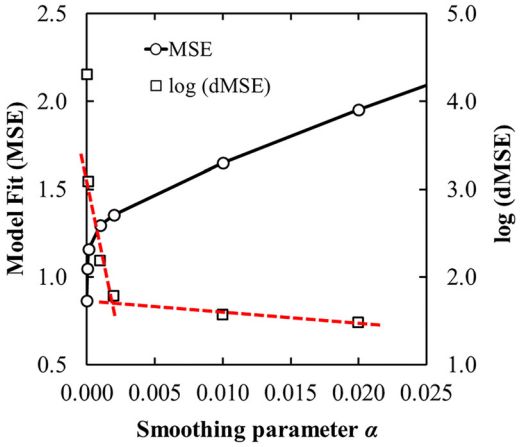

Figure 16: Profiles of MSE and logarithm of MSE difference quotient (the average rate of change) against the smoothing parameter α and determination the optimal α value using the L-method (see more details in Ref. [75]).

"leave-one-out" procedure (also sometimes abbreviated as OCV and LOOCV). Returning the removed data point to the data set and repeating this procedure for each data point yields certain prediction-error estimate for selected value of α. Then calculating an average error on a grid of possible values of parameter α, one can get some type of objective function CV(α) and choose the "best" value of α by minimizing (or maximizing) CV(α). However, despite its popularity and apparent simplicity the LOOCV procedure comes at the price of being computationally expensive, especially for data sets with large number of points, – usually, the "cost" of CV is of $O(N^2)$ where N denotes the sample size. Interested readers will find more details on the cross-validation based methods in Refs. [68, 99, 100]. Alternatively, one can use information-based criteria, like AIC or BIC, for the smoothing parameter selection. Multiple researchers conducted a comprehensive comparison of various smoothing parameter selection methods with different computational complexity (see, for instance, Refs. [101, 102]).

Also, as a naïve but practical procedure, one can use a simple graphical method, known as the "L-method" [103], for smoothing parameter selection. To illustrate that, we consider the results of SE data analysis for a thin metal layer of nickel-monosilicide (NiSi) [75]. The optical properties of the NiSi layer were represented by means of uniform B-splines with adjustable smoothing parameter. By performing the data fitting, we can plot MSE values and log-values of the MSE average rate of change as functions of the smoothing parameter α (Figure 16). As one can notice, the curves have two fairly flat regions on both the left and right sides and a highly-curved transition area in between. A case of $\alpha = 0$ corresponds to unpenalized dielectric function (see Equation (27)) and, therefore, the lowest MSE value (remember that a very large number of the B-spline functions has been used which resulted in very flexible B-spline curve). Both curves represent monotonic functions, either increasing or decreasing, and the bending point, where the rapidly changing functions MSE(α) and log(dMSE)(α) are transformed into slowly changing ones, is clearly visible (Figure 16). However, it is still not obvious how to objectively choose an appropriate, say, optimal value of the smoothing parameter beyond which the quality of fit ceases to deteriorate significantly. In order to determine the "best" value of α, the L-method fits a straight line to the points on one side, say, the left, of the graph and another line to the points on another side. An abscissa of the intersection of these lines will approximately indicate the required smoothing parameter value. The line fitting should be performed for all possible pairs of lines with different sequences of points by minimizing the total root-mean-squared error, i.e., the combined MSE for the lines at the left and right sides of the graph. Using the L-method, one can find the point of maximum curvature in the MSE average rate of change curve at $\alpha = 0.016$ which we accept as the optimal smoothing parameter value (Figure 16). The details of the analysis can be found in Ref. [75].

Here, we want to highlight that only the simplest case of P-spline formulation with a single, or global, smoothing parameter, – that is, the amount of smoothing of the dielectric function stays constant across the entire spectral region, – has been considered. However, in case of the complex-shaped dielectric functions, especially in a wide UV-VIS-NIR spectral range, an introduction of a variable smoothing parameter provides another possible way for P-spline modeling. In other words, a value of α may vary from one spectral region to another, for instance, based on a changing curve smoothness or derivative variations. Thus, further possible enhancement of the dielectric function representation by P-splines should also include a way for certain *adaptive smoothing* (see also Refs. [100, 104, 105] for more comprehensive details).

7 Concluding remarks

Dielectric function representation by various polynomial spline functions has now developed into an efficient method for accurate modeling of the material optical properties in the SE data analysis. This review discusses various ways of piecewise polynomial modeling of the dielectric function with emphasis on the B(asis)-spline functions. The history of the spline usage in a variety of

spectroscopic ellipsometry applications is about 30 years long, although for the purpose of data analysis (the curve fitting, in particular) in other fields of spectroscopy (e.g., Raman, electron and nuclear magnetic resonance spectroscopy, etc.) the splines have been used even earlier. And over the course of time, the area of B-spline applications in spectroscopy in general only expands into new practical fields such as, for instance, mid-infrared spectroscopy, imaging spectroscopy, gamma-ray spectra smoothing, time-resolved photoelectron spectroscopy, deformable image registration in medical image analysis and so on. As we describe in the preceding sections, there are multiple advantages in using the spline approximations for the dielectric function modeling. First of all, the DF spline representation allows an evaluation of the Kramers–Kronig transforms analytically and also guarantees physically reasonable results for the dielectric-function line shape. Now, although the DF parameterization by physics-based oscillator models allows direct determination of certain important parameters such as the critical points and bandgap energies, in industrial optical metrology there is often necessary to simply model the material optical properties for further thickness only measurements. And such a practically important task can be achieved successfully using various kinds of spline functions, without any prior knowledge on the optical properties of the material under test. Moreover, the spline approach should provide a potential for the SE analysis automation in the sense of recently published work by Oiwake et al. [106] to eliminate the need for expertise from high-level metrology specialist. Thus, we believe sincerely that the DF spline parameterization is an essential and fascinating concept that will continue to benefit the ellipsometric data modeling in the forthcoming years. Nevertheless, still more work is needed to implement already developed methods and algorithms of polynomial spline theory looking at the whole existing *zoo of splines*.

Acknowledgement: The author wishes to acknowledge the colleagues at GlobalFoundries Fab1 (Dresden, Germany) for their generous and constant support and succor. In particular, the assistance provided by Steffen Brunner, Sven Bürgel, Göran Fleischer, Thomas Kache, Ulf Peter Müller, and Pavel Prunici is appreciated.
Author contributions: The author has accepted responsibility for the entire content of this submitted manuscript and approved submission.
Research funding: None declared.
Conflict of interest statement: The author declare no conflicts of interest regarding this article.

References

[1] H. G. Tompkins and W. A. McGahan, *Spectroscopic Ellipsometry and Reflectometry: A User's Gide*, New York, John Wiley & Sons Inc., 1999.
[2] H. Fujiwara, *Spectroscopic Ellipsometry: Principles and Applications*, Chichester, West Sussex, U.K., John Wiley & Sons Ltd., 2007.
[3] H. G. Tompkins and J. N. Hilfiker, *Spectroscopic Ellipsometry: Practical Application to Thin Film Characterization*, New York, Momentum Press, 2016.
[4] R. W. Collins and A. S. Ferlauto, "Optical physics of materials," in *Handbook of Ellipsometry*, Norwich, NY, USA, William Andrew Publishing/Noyes, 2005, pp. 93–235.
[5] J. N. Hilfiker and T. Tiwald, "Dielectric function modeling," in *Spectroscopic Ellipsometry for Photovoltaics: Fundamental Principles and Solar cell Characterization*, vol. 1, Cham, Switzerland, Springer-Verlag, 2018, pp. 115–153.
[6] I. J. Schoenberg, "Contributions to the problem of approximation of equidistant data by analytic functions.–Part A. On the problem of smoothing or graduation. A first class of analytic approximation formulae," *Q. Appl. Math.*, vol. 4, pp. 45–99, 1946.
[7] I. J. Schoenberg, "Contributions to the problem of approximation of equidistant data by analytic functions.–Part B. On the problem of osculatory interpolation. A second class of analytic approximation formulae," *Q. Appl. Math.*, vol. 4, pp. 112–141, 1946.
[8] L. D. Landau, E. M. Lifshitz, and L. P. Pitaevskii, *Electrodynamics of Continuous Media*, 2nd ed. Amsterdam, The Netherlands, Elsevier Butterworth-Heinemann, 1984.
[9] R. Courant and D. Hilbert, *Methods of Mathematical Physics*, vol. I, Berlin, Wiley-VCH, 1989.
[10] J. K. Jerome, *Three Men in a Boat and Three Men On The Bummel (Oxford World's Classics)*, New York, Oxford University Press, 1998.
[11] C. Runge, "Über empirische Funktionen und die Interpolation zwischen äquidistanten Ordinaten," *Z. Math. Phys.*, vol. 46, pp. 224–243, 1901.
[12] H. A. Buchdahl, *Optical Aberration Coefficients*, Mineola, NY, U.S.A., Dover Publications, Inc., 1968.
[13] J. H. Ahlberg, E. N. Nilson, and J. L. Walsh, *The Theory of Splines and Their Applications*, New York, Academic Press, Inc., 1967.
[14] L. L. Schumaker, *Spline Functions: Basic Theory*, 3rd ed. Cambridge, U.K., Cambridge University Press, 2007.
[15] P. Dierckx, *Curve and Surface Fitting with Splines*, New York, Oxford University Press, 1993.
[16] J. D. Brown, *Advanced Statistics for The Behavioral Sciences: A Computational Approach with R*, Cham, Switzerland, Springer, 2018.
[17] I. J. Schoenberg, "On interpolation by spline functions and its minimal properties," in *On Approximation Theory/über Approximationstheorie: Proceedings of The Conference Held in the Mathematical Research Institute*, P. L. Butzer, and J. Korevaar, Eds., Basel, Springer-Verlag, 1964, pp. 109–129. Oberwolfach, Black Forest, August 4–10, 1963.
[18] H. Akima, "A new method of interpolation and smooth curve fitting based on local procedures," *J. ACM*, vol. 17, pp. 589–602, 1970.

[19] J. Fried and S. Zietz, "Curve fitting by spline and Akima methods: Possibility of interpolation error and its suppression," *Phys. Med. Biol.*, vol. 18, pp. 550–558, 1973.
[20] M. Steffen, "A simple method for monotonic interpolation in one dimension," *Astron. Astrophys.*, vol. 239, pp. 443–450, 1990.
[21] C. Moler, "Makima piecewise cubic interpolation, cleve's corner: Cleve moler on mathematics and computing," Available at: https://blogs.mathworks.com/cleve/2019/04/29/makima-piecewise-cubic-interpolation/#d9a97978-0b09-4a1f-a6a5-504d088631d0 [accessed: Feb. 22, 2022].
[22] C. de Boor, *A Practical Guide to Splines*, Revised Edition, New York, Springer-Verlag, 2001.
[23] C. de Boor, "On calculating with B-splines," *J. Approx. Theor.*, vol. 6, pp. 50–62, 1972.
[24] M. G. Cox, "The numerical evaluation of B-splines," *IMA J. Appl. Math.*, vol. 10, pp. 134–149, 1972.
[25] C. de Boor and A. Pinkus, "The B-spline recurrence relations of Chakalov and of Popoviciu," *J. Approx. Theor.*, vol. 124, pp. 115–123, 2003.
[26] T. Lyche, C. Manni, and H. Speleers, "Foundations of spline theory: B-splines, spline approximation, and hierarchical refinement," in *Splines and PDEs: From Approximation Theory to Numerical Linear Algebra, Lecture Notes in Mathematics*, vol. 2219, Cham, Switzerland, Springer, 2018, pp. 1–76.
[27] J. R. Rice, *Numerical Methods in Software and Analysis*, 2nd ed. San Diego, Academic Press, 1993.
[28] B. Johs and J. S. Hale, "Dielectric function representation by B-splines," *Phys. Status Solidi*, vol. 205, pp. 715–719, 2008.
[29] I. Failes, "The tech of 'Terminator 2' – an oral history, October 21, 2019, *befores & afters* visual effects and animation online magazine," Available at: https://beforesandafters.com/2019/10/21/the-tech-of-terminator-2-an-oral-history/ [accessed: Feb. 22, 2022].
[30] J.-T. Zettler, M. Weidner, and A. Röseler, "On the characterization of silicon dioxide and silicon nitride by spectroscopic ellipsometry in the VIS and IR regions," *Phys. Status Solidi*, vol. 124, pp. 547–555, 1991.
[31] J. Vanhellemont and H. E. Maes, "Spectroscopic ellipsometry characterization of silicon-on-insulator materials," *Mater. Sci. Eng. B*, vol. 5, pp. 301–307, 1990.
[32] J. Vanhellemont, P. Roussel, and H. E. Maes, "Spectroscopic ellipsometry for depth profiling of ion implanted materials," *Nucl. Instrum. Methods Phys. Res. B*, vol. 55, pp. 183–187, 1991.
[33] J. Vanhellemont and P. Roussel, "Characterization by spectroscopic ellipsometry of buried layer structures in silicon formed by ion beam synthesis," *Mater. Sci. Eng. B*, vol. 12, pp. 165–172, 1992.
[34] Y. Z. Hu, J.-T. Zettler, S. Chongsawangvirod, Y. Q. Wang, and E. A. Irene, "Spectroscopic ellipsometric measurements of the dielectric function of germanium dioxide films on crystal germanium," *Appl. Phys. Lett.*, vol. 61, pp. 1098–1100, 1992.
[35] J.-T. Zettler, T. Trepk, L. Spanos, Y.-Z. Hu, and W. Richter, "High precision UV-visible-near-IR Stokes vector spectroscopy," *Thin Solid Films*, vol. 234, pp. 402–407, 1993.
[36] D. Zwillinger, *Handbook of Integration*, Boston, London, Jones and Bartlett Publishers, 1992.
[37] A. P. Prudnikov, Y. A. Brychkov, and O. I. Marichevin, *Integrals and Series: Elementary Functions*, vol. 1, New York, London, Gordon & Breach Science Publishers, 1986.
[38] M. Zorn, T. Trepk, J.-T. Zettler, et al., "Temperature dependence of the InP(001) bulk and surface dielectric function," *Appl. Phys. A*, vol. 65, pp. 333–339, 1997.
[39] D. De Sousa Meneses, B. Rousseau, P. Echegut, and G. Matzen, "Piecewise polynomial dielectric function model and its application for the retrieval of optical functions," *Appl. Spectrosc.*, vol. 61, pp. 644–648, 2007.
[40] M. Gilliot, A. Hadjadj, and M. Stchakovsky, "Spectroscopic ellipsometry data inversion using constrained splines and application to characterization of ZnO with various morphologies," *Appl. Surf. Sci.*, vol. 421, pp. 453–459, 2017.
[41] M. Gilliot, "Inversion of ellipsometry data using constrained spline analysis," *Appl. Opt.*, vol. 56, pp. 1173–1182, 2017.
[42] C. C. Kim, J. W. Garland, H. Abad, and P. M. Raccah, "Modeling the optical dielectric function of semiconductors: extension of the critical-point parabolic-band approximation," *Phys. Rev. B*, vol. 45, pp. 11749–11767, 1992.
[43] C. C. Kim, J. W. Garland, and P. M. Raccah, "Modeling the optical dielectric function of the alloy system Al*x*Ga1–*x*As," *Phys. Rev. B*, vol. 47, pp. 1876–1888, 1993.
[44] S. H. Han, S. Yoo, B. Kippelen, and D. Levi, "Precise determination of optical properties of pentacene thin films grown on various substrates: Gauss–Lorentz model with effective medium approach," *Appl. Phys. B*, vol. 104, pp. 139–144, 2011.
[45] B. Johs, C. M. Herzinger, J. H. Dinan, A. Cornfeld, and J. D. Benson, "Development of a parametric optical constant model for $Hg_{1-x}Cd_xTe$ for control of composition by spectroscopic ellipsometry during MBE growth," *Thin Solid Films*, vols. 313–314, pp. 137–142, 1998.
[46] C. M. Herzinger, B. Johs, W. A. McGahan, and J. A. Woollam, "Ellipsometric determination of optical constants for silicon and thermally grown silicon dioxide via a multi-sample, multi-wavelength, multi-angle investigation," *J. Appl. Phys.*, vol. 83, pp. 3323–3336, 1998.
[47] E. Franke, C. L. Trimble, M. J. DeVries, J. A. Woollam, M. Schubert, and F. Frost, "Dielectric function of amorphous tantalum oxide from the far infrared to the deep ultraviolet spectral region measured by spectroscopic ellipsometry," *J. Appl. Phys.*, vol. 88, pp. 5166–5174, 2000.
[48] L. Yan, J. A. Woollam, and E. Franke, "Oxygen plasma effects on optical properties of ZnSe films," *J. Vac. Sci. Technol. A*, vol. 20, pp. 693–701, 2002.
[49] T. J. Kim, T. H. Ghong, Y. D. Kim, et al., "Dielectric functions of In_xGa_{1-x} As alloys," *Phys. Rev. B*, vol. 68, p. 115323, 2003.
[50] V. R. D'Costa, C. S. Cook, A. G. Birdwell, et al., "Optical critical points of thin-film $Ge_{1-y}Sn_y$ alloys: a comparative $Ge_{1-y}Sn_y$/$Ge_{1-x}Si_x$ study," *Phys. Rev. B*, vol. 73, p. 125207, 2006.
[51] E. Agocs, B. Fodor, et al., "Approaches to calculate the dielectric function of ZnO around the band gap," *Thin Solid Films*, vol. 571, pp. 684–688, 2014.
[52] C. Xu, J. D. Gallagher, C. L. Senaratne, J. Menéndez, and J. Kouvetakis, "Optical properties of Ge-rich $Ge_{1-x}Si_x$ alloys: Compositional dependence of the lowest direct and indirect gaps," *Phys. Rev. B*, vol. 93, p. 125206, 2016.
[53] V. L. Le, T. J. Kim, H. G. Park, H. T. Nguyen, X. A. Nguyen, and Y. D. Kim, "Temperature dependence of the dielectric function of monolayer MoS_2," *Curr. Appl. Phys.*, vol. 19, pp. 182–187, 2019.

[54] A. B. Kuzmenko, "Kramers–Kronig constrained variational analysis of optical spectra," *Rev. Sci. Instrum.*, vol. 76, p. 083108, 2005.
[55] J. Levallois, I. O. Nedoliuk, I. Crassee, and A. B. Kuzmenko, "Magneto-optical Kramers–Kronig analysis," *Rev. Sci. Instrum.*, vol. 86, p. 033906, 2015.
[56] J. W. Weber, T. A. R. Hansen, M. C. M. van de Sanden, and R. Engeln, "B-spline parametrization of the dielectric function applied to spectroscopic ellipsometry on amorphous carbon," *J. Appl. Phys.*, vol. 106, p. 123503, 2009.
[57] L. S. Abdallah, S. Zollner, C. Lavoie, A. Ozcan, and M. Raymond, "Compositional dependence of the optical conductivity of $Ni_{1-x}Pt_x$ alloys ($0 < x < 0.25$) determined by spectroscopic ellipsometry," *Thin Solid Films*, vol. 571, pp. 484–489, 2014.
[58] R. Schmidt-Grund, C. Kranert, H. von Wenckstern, V. Zviagin, M. Lorenz, and M. Grundmann, "Dielectric function in the spectral range (0.5–8.5) eV of an $(Al_xGa_{1-x})_2O_3$ thin film with continuous composition spread," *J. Appl. Phys.*, vol. 117, p. 165307, 2015.
[59] V. Zviagin, P. Richter, T. Böntgen, et al., "Comparative study of optical and magneto-optical properties of normal, disordered, and inverse spinel-type oxides," *Phys. Status Solidi B*, vol. 253, pp. 429–436, 2016.
[60] P. Petrik, A. Sulyok, T. Novotny, et al., "Optical properties of Zr and ZrO_2," *Appl. Surf. Sci.*, vol. 421, pp. 744–747, 2017.
[61] S. Schöche, N. Hong, M. Khorasaninejad, et al., "Optical properties of graphene oxide and reduced graphene oxide determined by spectroscopic ellipsometry," *Appl. Surf. Sci.*, vol. 421, pp. 778–782, 2017.
[62] J. Sun and G. K. Pribil, "Analyzing optical properties of thin vanadium oxide films through semiconductor-to-metal phase transition using spectroscopic ellipsometry," *Appl. Surf. Sci.*, vol. 421, pp. 819–823, 2017.
[63] S. Prucnal, Y. Berencén, M. Wang, et al., "Strain and band-gap engineering in Ge-Sn alloys via P doping," *Phys. Rev. Applied*, vol. 10, p. 064055, 2018.
[64] S. Prucnal, Y. Berencén, M. Wang, et al., "Band gap renormalization in n-type GeSn alloys made by ion implantation and flash lamp annealing," *J. Appl. Phys.*, vol. 125, p. 203105, 2019.
[65] S. Richter, O. Herrfurth, S. Espinoza, et al., "Ultrafast dynamics of hot charge carriers in an oxide semiconductor probed by femtosecond spectroscopic ellipsometry," *New J. Phys.*, vol. 22, p. 083066, 2020.
[66] J. Mohrmann, T. E. Tiwald, J. S. Hale, J. N. Hilfiker, and A. C. Martin, "Application of a B-spline model dielectric function to infrared spectroscopic ellipsometry data analysis," *J. Vac. Sci. Technol. B*, vol. 38, p. 014001, 2020.
[67] V. Zviagin, M. Grundmann, and R. Schmidt-Grund, "Impact of defects on magnetic properties of spinel zinc ferrite thin films," *Phys. Status Solidi B*, vol. 257, p. 1900630, 2020.
[68] P. H. C. Eilers and B. D. Marx, *Practical Smoothing: The Joys of P-Splines*, Cambridge, UK, Cambridge University Press, 2021.
[69] J. Schelten and F. Hossfeld, "Application of spline functions to the correction of resolution errors in small-angle scattering," *J. Appl. Crystallogr.*, vol. 4, pp. 210–223, 1971.
[70] O. Glatter, "A new method for the evaluation of small-angle scattering data," *J. Appl. Crystallogr.*, vol. 10, pp. 415–421, 1977.
[71] J. S. Pedersen, "Model-independent determination of the surface scattering-length-density profile from specular reflectivity data," *J. Appl. Crystallogr.*, vol. 25, pp. 129–145, 1992.
[72] N. F. Berk and C. F. Majkrzak, "Using parametric B splines to fit specular reflectivities," *Phys. Rev. B*, vol. 51, pp. 11296–11309, 1995.
[73] D. V. Likhachev, "Selecting the right number of knots for B-spline parameterization of the dielectric functions in spectroscopic ellipsometry data analysis," *Thin Solid Films*, vol. 636, pp. 519–526, 2017.
[74] D. V. Likhachev, "B-spline parameterization of the dielectric function and information criteria: the craft of non-overfitting," in *Modeling Aspects in Optical Metrology VI*, B. Bodermann, K. Frenner, and R. M. Silver, Eds., Munich, Germany, June 25–29, 2017, SPIE Proc. 10330, 2017, p. 103300B.
[75] D. V. Likhachev, "Spectroscopic ellipsometry data analysis using penalized splines representation for the dielectric function," *Thin Solid Films*, vol. 669, pp. 174–180, 2019.
[76] D. V. Likhachev, "A practitioner's approach to evaluation strategy for ellipsometric measurements of multilayered and multiparametric thin-film structures," *Thin Solid Films*, vol. 595, pp. 113–117, 2015.
[77] D. V. Likhachev, "Model selection in spectroscopic ellipsometry data analysis: combining an information criteria approach with screening sensitivity analysis," *Appl. Surf. Sci.*, vol. 421, pp. 617–623, 2017.
[78] A. Jogalekar, "Derek Lowe to world: "Beware of von Neumann's elephants," 2015. Available at: http://wavefunction.fieldofscience.com/2015/02/derek-lowe-to-world-beware-of-von.html [accessed: Jan. 11, 2022].
[79] F. Dyson, "A meeting with Enrico Fermi," *Nature (London)*, vol. 427, p. 297, 2004.
[80] J. Mayer, K. Khairy, and J. Howard, "Drawing an elephant with four complex parameters," *Am. J. Phys.*, vol. 78, pp. 648–649, 2010.
[81] K. P. Burnham and D. Anderson, *Model Selection and Multimodel Inference: A Practical Information-Theoretic Approach*, 2nd ed. New York, Springer-Verlag, 2002.
[82] D. V. Likhachev, "On the optimization of knot allocation for B-spline parameterization of the dielectric function in spectroscopic ellipsometry data analysis," *J. Appl. Phys.*, vol. 129, p. 034903, 2021.
[83] V. T. Dung and T. Tjahjowidodo, "A direct method to solve optimal knots of B-spline curves: an application for non-uniform B-spline curves fitting," *PLoS ONE*, vol. 12, p. e0173857, 2017.
[84] P. Laube, M. O. Franz, and G. Umlauf, "Learnt knot placement in B-spline curve approximation using support vector machines," *Comput. Aided Geomet. Des.*, vol. 62, pp. 104–116, 2018.
[85] R. Yeh, Y. S. G. Nashed, T. Peterka, and X. Tricoche, "Fast automatic knot placement method for accurate B-spline curve fitting," *Comput. Aided Des.*, vol. 128, p. 102905, 2020.
[86] D. Michel and A. Zidna, "A new deterministic heuristic knots placement for B-spline approximation," *Math. Comput. Simulat.*, vol. 186, pp. 91–102, 2021.
[87] D. Lenz, O. Marin, V. Mahadevan, R. Yeh, and T. Peterka, "Fourier-informed knot placement schemes for B-spline approximation", preprint arXiv: 2012.04123 [math.NA], 2020.

[88] D. L. B. Jupp, "Approximation to data by splines with free knots," *SIAM J. Numer. Anal.*, vol. 15, pp. 328–343, 1978.
[89] T. J. Jacobson and M. J. Murphy, "Optimized knot placement for B-splines in deformable image registration," *Med. Phys.*, vol. 38, pp. 4579–4582, 2011.
[90] D. R. Forsey and R. H. Bartels, "Hierarchical B-spline refinement," *ACM SIGGRAPH Comput. Graph.*, vol. 22, pp. 205–212, 1988.
[91] C. Giannelli, B. Jüttler, and H. Speleers, "THB-splines: The truncated basis for hierarchical splines," *Comput. Aided Geomet. Des.*, vol. 29, pp. 485–498, 2012.
[92] K. A. Johannessen, F. Remonato, and T. Kvamsdal, "On the similarities and differences between classical hierarchical, truncated hierarchical and LR B-splines," *Comput. Methods Appl. Mech. Eng.*, vol. 291, pp. 64–101, 2015.
[93] C. Conti, R. Morandi, C. Rabut, and A. Sestini, "Cubic spline data reduction choosing the knots from a third derivative criterion," *Numer. Algorithm.*, vol. 28, pp. 45–61, 2001.
[94] A. N. Tikhonov and V. Y. Arsenin, *Solutions of Ill-Posed Problems*, Washington, D.C., V. H. Winston & Sons, 1977.
[95] A. G. Yagola, "Ill-posed problems and methods for their numerical solution," in *Optimization and Regularization for Computational Inverse Problems and Applications*, Berlin, Heidelberg, Springer, 2010, pp. 17–34.
[96] F. O'Sullivan, "A statistical perspective on ill-posed inverse problems (with discussion)," *Stat. Sci.*, vol. 1, pp. 502–527, 1986.
[97] P. H. C. Eilers and B. D. Marx, "Flexible smoothing with B-splines and penalties," *Stat. Sci.*, vol. 11, pp. 89–102, 1996.
[98] P. H. C. Eilers, B. D. Marx, and M. Durbán, "Twenty years of P-splines," *SORT-Stat. Oper. Res. Trans.*, vol. 39, pp. 149–186, 2015.
[99] G. Wahba, *Spline Models for Observational Data*, Philadelphia, PA, SIAM: Society for Industrial and Applied Mathematics, 1990.
[100] D. Ruppert, M. P. Wand, and R. J. Carroll, *Semiparametric Regression*, Cambridge, UK, Cambridge University Press, 2003.
[101] T. C. M. Lee, "Smoothing parameter selection for smoothing splines: A simulation study," *Comput. Stat. Data Anal.*, vol. 42, pp. 139–148, 2003.
[102] L. N. Berry and N. E. Helwig, "Cross-validation, information theory, or maximum likelihood? A comparison of tuning methods for penalized splines," *Stats*, vol. 4, no. 2021, pp. 701–724.
[103] S. Salvador and P. Chan, "Learning states and rules for detecting anomalies in time series," *Appl. Intell.*, vol. 23, pp. 241–255, 2005.
[104] A. A. Urbas and S. J. Choquette, "Automated spectral smoothing with spatially adaptive penalized least squares," *Appl. Spectrosc.*, vol. 65, pp. 665–677, 2011.
[105] X. Wang, P. Du, and J. Shen, "Smoothing splines with varying smoothing parameter," *Biometrika*, vol. 100, pp. 955–970, 2013.
[106] K. Oiwake, Y. Nishigaki, S. Fujimoto, S. Maeda, and H. Fujiwara, "Fully automated spectroscopic ellipsometry analyses: application to MoO_x thin films," *J. Appl. Phys.*, vol. 129, p. 243102, 2021.

Bionote

Dmitriy V. Likhachev
GlobalFoundries Dresden Module One LLC & Co. KG, Wilschdorfer Landstr. 101, D-01109 Dresden, Germany
dmitriy.likhachev@globalfoundries.com
https://orcid.org/0000-0002-9842-528X
Dmitriy V. Likhachev began his studies in Technical Physics at the S.M. Kirov Ural Polytechnic Institute (Sverdlovsk, U.S.S.R.) in 1980 and received his Ph.D. in Solid State Physics (Candidate of Science) from the Ural State Technical University (Ekaterinburg, Russia) in 1993. He is currently a Member of Technical Staff with GlobalFoundries (Dresden, Germany). His present interests include applications of spectroscopic ellipsometry to material characterization and process control in semiconductor development and manufacturing.